JOURNAL OF GEOPHYSICAL RESEARCH, VOL. 107, NO. D16, 10.1029/2001JD001015, 2002

Denitrification inside the stratospheric vortex in the winter of 1999–2000 by sedimentation of large nitric acid trihydrate particles

Harald Flentje, Andreas Dörnbrack, Andreas Fix, Alexander Meister, and Heidi Schmid
Institut für Physik der Atmosphäre, Deutsches Zentrum für Luft- und Raumfahrt Oberpfaffenhofen, Wessling, Germany

Stefan Füglistaler, Beiping Luo, and Thomas Peter
Laboratorium für Atmosphärenphysik, Eidgenossische Technische Hochschule, Zürich, Zürich, Switzerland

Received 2 July 2001; revised 3 December 2001; accepted 17 December 2001; published 29 August 2002.

[1] Synoptic-scale polar stratospheric clouds (PSCs) have been measured with an aircraft-borne lidar south of Spitsbergen in early February 2000. The PSCs of moderately depolarizing stratified layers extended from near the tropopause (10–11 km) up to 20 km altitude. Their internal structure in backscatter ratio reflects the variability of the particles' concentration rather than manifold sizes and phases of different optical efficiency. Actually, their size distribution was nearly monodisperse. According to T-matrix calculations, low backscatter ratios ($\gamma < 3$), color ratios of 1–1.5, and moderate depolarization ratios ($\delta_a \approx 0.15-0.2$) indicate that the observed layers were composed of aspherical nitric acid trihydrate (NAT) particles larger than 2 μm. During three turning point missions into the cold vortex core a significant settling of the particle layers was observed between aligned outgoing and incoming legs. Low stratospheric winds and quasi-Lagrangian flight heading minimized horizontal drifts between the probed volumes. A NAT particle sedimentation velocity of 69 ± 14 m/h is derived by cross-covariance analysis of corresponding pairs of two-dimensional backscatter sections of the layers. This implies a particle size of $r_p \approx 7-8$ μm and a mixing ratio of condensed HNO_3 near 2 ppbv. The downward NO_y flux below 19 km altitude amounts to $j \approx 3$ ppbv km/d. Based on particle back trajectory analysis, this flux, derived from the observations in different regions of the Northern European Ice Sea, has a significant denitrification potential. *INDEX TERMS:* 0341 Atmospheric Composition and Structure: Middle atmosphere—constituent transport and chemistry (3334); 0305 Atmospheric Composition and Structure: Aerosols and particles (0345, 4801); 0320 Atmospheric Composition and Structure: Cloud physics and chemistry; 1610 Global Change: Atmosphere (0315, 0325); *KEYWORDS:* airborne lidar, polar stratospheric clouds, denitrification, nitric acid trihydrate

1. Motivation

[2] The chemical ozone depletion inside the Arctic stratosphere during single winters is largely determined by the abundance of polar stratospheric cloud (PSC) particles: First, as locations of heterogeneous conversion of inert reservoir gases ($ClNO_3$, HCl, HNO_3, ...) into active chlorine radicals (ClO_x) which under sunlight drive the catalytic ozone destruction cycle [*Solomon et al.*, 1986]. Second, the particles incorporate $HNO_{3,g} \rightarrow HNO_{3,cond.}$, the source of NO_2, from the gas phase and thereby reduce the repassivation of the active forms via the $ClO + NO_2 + M \rightarrow ClONO_2 + M$ reaction [*Solomon*, 1990; *Fahey et al.*, 1990; *Rex et al.*, 1997]. NO_x (= NO + NO_2) is converted into $HNO_{3,g}$ via particle-surface-catalyzed reactions (denoxification). If persistent gas to particle conversion allows the particles to grow to sizes larger than a few micrometers their gravitational sedimentation becomes relevant in the course of their life time. A downward HNO_3-flux (and thereby a downward NO_y-flux - NO_y usually includes NO, NO_2, NO_3, N_2O_5, $ClONO_2$, HNO_3, HNO_4) establishes and leads to a permanent removal of nitrogen from higher stratospheric layers (denitrification) and simultaneous injection into the layers below (nitrification), where the falling particles re-evaporate [*Hübler et al.*, 1990; *Kawa et al.*, 1992; *Waibel et al.*, 1999; *Kondo et al.*, 2000]. The growth rate of HNO_3-containing PSC particles is strongly anticorrelated with temperature. Therefore, above Antarctica, where temperatures persistently fall below the temperature threshold for ice PSC formation (T_{ice}), strong denitrification regularly occurs while in the Arctic stratosphere, where temperatures typically range around the nitric acid trihydrate (NAT) saturation level T_{NAT}, denitrification had rarely become significant in the last winters. However, recent sensitivity studies by *Shindell et al.* [1998] and *Waibel et al.* [1999] indicate that the Arctic stratosphere currently is at the

0148-0227/02/2001JD001015$09.00

temperature threshold for denitrification. This implies that future stratospheric cooling, for example resulting from anthropogenic greenhouse forcing, would favor PSC formation and intensify denitrification, leading to a prolonged ozone destruction in the boreal late winter/early spring. In some winters like in 1994–1995, denitrification accounted for more than 30% of the total Arctic ozone loss, and more than 80% of the observed NO_y-deficit was due to sedimenting particles [*Waibel et al.*, 1999]. Over Antarctica, ice particles can grow to large sizes and effectively dehydrate and simultaneously denitrify the stratosphere [*Kelly et al.*, 1989; *Vömel et al.*, 1995], as $HNO_{3,g}$ (as NAT) is incorporated into ice particles. Against this, in the Arctic, pronounced dehydration is rarely observed [*Kelly et al.*, 1990; *Randel et al.*, 1998] owing to either warmer temperatures and/or stronger gravity wave activities which leads to much higher ice particle densities and thus limits the size of the ice particles. Only recently, during the very cold winters of 1994–1995 and 1995–1996, dehydration has been documented for single events [*Hintsa et al.*, 1998; *Stowasser et al.*, 1999] or in 1999–2000 even on larger scales [*Schiller et al.*, 2002]. Very large NAT particles with radii up to 10 μm have been detected in the 2000–2001 winter with an airborne NO_y-instrument [*Fahey et al.*, 2001] and a Multiangle Aerosol Spectrometer Probe (MASP) (S. D. Brooks et al., manuscript in preparation, 2002). A number of future laboratory and field studies will address the understanding of the link between denitrification and dehydration.

[3] During recent Arctic winters, frequently PSCs were observed which had formed temporarily in gravity waves, where air masses flowing across a mountain ridge experienced rapid adiabatic cooling occasionally by more than 10 K [*Carslaw et al.*, 1998; *Dörnbrack et al.*, 2002]. In this quasi-stationary process particles form and evaporate on relatively short timescales of a few hours. Correspondingly, small NAT particles with high number densities occur at these locations, which do not sediment significantly by gravity. In this paper we report observations of widespread large NAT particles with very low number density, the formation mechanism of which is quite unclear. To grow to the observed large sizes, these NAT particles must have stayed at least 3–5 days in air masses supersaturated with respect to NAT. According to ECMWF analyses this precondition is fulfilled for the observations presented in the following. Extended synoptic-scale PSCs only occur in winters with an exceptionally stable and cold vortex like in 1994–1995, 1995–1996 and in 1999–2000 when the large NASA-sponsored SAGE III Ozone Loss and Validation Experiment (SOLVE) and the European-Union-sponsored Third European Stratospheric Experiment on Ozone (THESEO-2000) campaigns took place. During this winter, various ground-based, balloon-borne and aircraft-borne measurements of gases and particles, both remote and in situ, were performed with efforts concentrated to three intense observation phases in early, high and late winter. The measurements we refer to took place during the second deployment from mid-January to early February.

[4] The paper is organized as follows: The next section provides an overview of the instrument, its employment and the fundamentals of our analysis. Section 3 describes the lidar observations in the light of particle sedimentation and synoptic meteorological analyses. The implications are then discussed and summarized in sections 4 and 5.

2. Experimental and Analytical Methods

2.1. Lidar

[5] Experimental data presented below have been measured by means of an aircraft-borne lidar during the second SOLVE deployment, on 31 January and 2 and 3 February 2000. The first two flights went directly from Kiruna (north Sweden, 68°N, 21°E) to western Spitsbergen (≈ 80°N, 11°E). The third mission went from Kiruna via the North Cape directing toward the Bear Island and returned at 73°N. On all flights the outbound and inbound legs were colocated as shown in Figure 1. During the campaign the aerosol-ozone lidar OLEX was installed on board the DLR research aircraft Falcon 20. It employs the fundamental, second and third harmonic radiation of a Nd:YAG laser corresponding to wavelengths of 1064 nm, 532 nm and 355 nm, respectively [*Wirth and Renger*, 1996; *Flentje et al.*, 2000]. Depolarization is measured at 532 nm. The back-scattered radiation is received by a 35 cm diameter Cassegrain telescope. With a repetition rate of 10 Hz for a typical aircraft speed of 200 m/s the raw data resolution is about 20 m in the horizontal. In the vertical, the ADC sampling rate results in a resolution of 15 m. The single profiles are averaged horizontally and vertically, resulting in a trade-off between error and spatial resolution. The (total) backscatter ratio, denoted by γ, is defined as the ratio of the total backscatter coefficient to the molecular backscatter coefficient $\gamma = (\beta_{particles} + \beta_{molecules})/\beta_{molecules}$. For the inversion of the β-profiles the standard Klett method was applied [*Klett*, 1985]. In order to maintain the high spatial resolution, however, the 2-D sections used for the sedimentation analysis are not corrected for extinction (i.e., not Klett-inverted), which introduces only a negligible error of less than 10^{-3} in the backscatter ratio. From the backscatter coefficients at the three wavelengths two color ratios are derived as indicators for the optically dominating effective particle size. The particle depolarization at 532 nm $\delta_{p,532} = \beta_{p,\perp}/\beta_{p,\|}$, where $\|$ and $\perp$ denote parallel and perpendicularly polarized radiation, provides information on the particles' shapes or phase (liquid/solid). A powerful analytical method to derive microphysical particle properties from the lidar data is the T-matrix approach [*Mishchenko*, 1991; *Macke et al.*, 1995]. It allows the analytical calculation of backscatter cross sections for axially symmetric particles of different sizes, shapes and compositions parametrized by their complex refractive index. The applicability of this method to PSC particles has been recently confirmed by studies of, e.g., *Carslaw et al.* [1998] and *Wirth et al.* [1999] assuming a spheroid geometry. Once having generated a set of lookup tables for the lidar parameters, namely backscatter ratios γ_{1064nm}, γ_{532nm}, γ_{355nm}, (corresponding to two "color ratios") and the depolarization ratio $\delta_{532\ nm}$, the particle properties (effective radius r_{eff} and aspect ratio) that are compatible with the lidar observations can quickly be derived. After all available optical data is taken into account, ambiguities may still remain but in many cases can be ruled out by plausibility arguments or

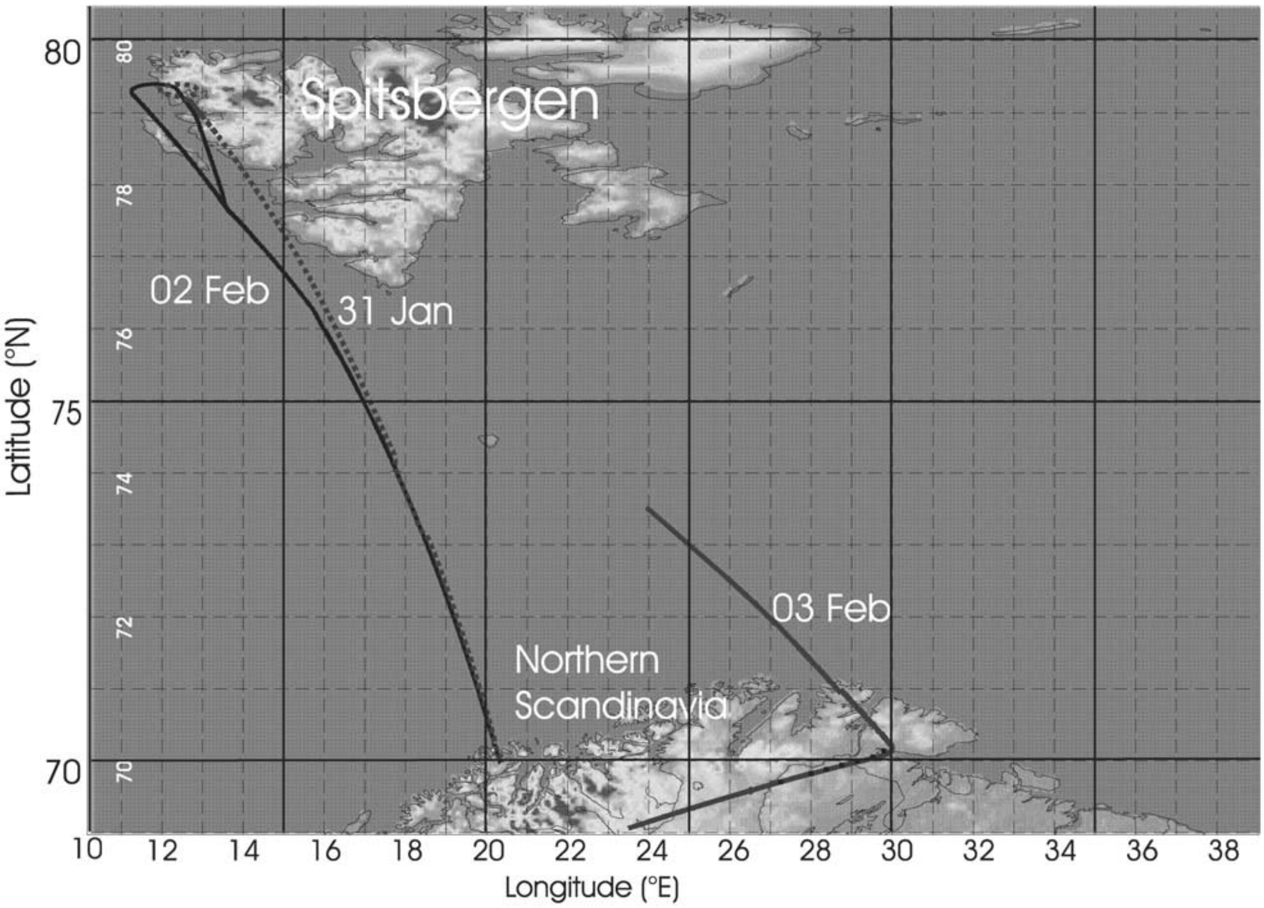

Figure 1. Falcon flight paths on 31 January 2000 (1030–1230 UT) and 2 February (1330–1505 UT) and 3 February 2000 (1940–2015 UT) over the Northern European Ice Sea south of Spitsbergen. Color-coded elevation shows peak altitudes of more than 1000 m above sea level. See color version of this figure at back of this issue.

independent information from other sources. For arbitrarily shaped particles, ray tracing techniques may also be applied.

2.2. Meteorological Situation

[6] The winter of 1999–2000 belongs to the coldest winters in the lower stratosphere within the last 30 years. The Arctic vortex stayed cold with extremely low mean temperatures at 30 to 50 hPa and persistent PSC occurrence from mid-November until March. Negative temperature deviations of $-12°$ to $-15°C$ at 30 hPa were analyzed over long times and large areas [*Naujokat et al.*, 2000; *Manney and Sabutis*, 2000]. During the time of the measurements in late January and early February a strong, cold vortex with its center over Spitsbergen dominated the stratospheric circulation. The coldest air with synoptic temperatures below 190 K covered the Arctic Sea and extended from the east coast of Greenland to north of Siberia (see Figures 2a–2c). The vortex edge run nearly zonally over northern Europe and was marked by a strong meridional wind speed gradient between 60°N and 70°N. During the campaign the vortex edge slowly swept westward over northern Europe accompanied by a turn of the stratospheric wind from westerlies to northwesterlies in the observation area. PSC-level winds in the vicinity of the flight track south of Spitsbergen calmed during the period and were lower in the north. Horizontal velocities between 2–5 m/s were analyzed by the ECMWF in that region (Figures 2d–2f). The vertical wind, derived as a residual of the balanced quasi geostrophic flow, ranged from -0.5 cm/s on 31 January to near zero on 2 February and about +0.3 cm/s on 3 February near the edges of the respective PSCs. A trajectory analysis shows that it took less than 5 days for the air masses to circulate once around the vortex. Before 3 February all particle trajectories (referred to 5–9 μm particles) north of 76°N cross Greenland in a cyclonic flow. Those north of about 72°N at the observation time had stayed around the NAT saturation temperature for at least 2 days before 2 February. The particles probed on 3 February were confined to the center of the vortex for about a week and remained below NAT temperatures for 4 days.

2.3. Sedimentation Analysis

[7] The sedimentation velocity w_p of stratospheric particles which are decelerated by viscous friction is a function of their radius, density and shape. Thus, if referred to the surrounding air it allows to determine these

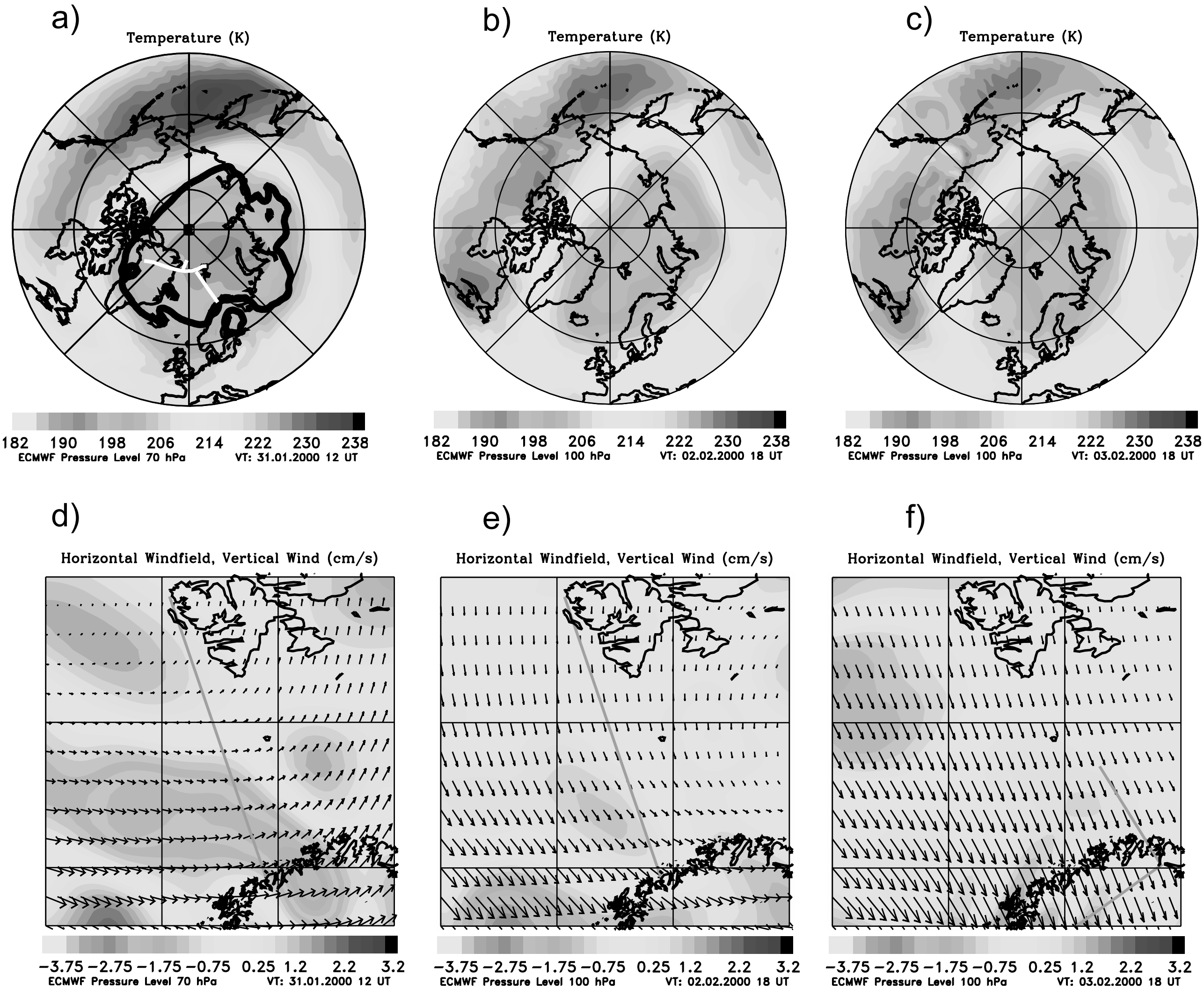

Figure 2. Upper panels: ECMWF temperatures at 70 hPa on (a) 31 January 1200 UT and at 100 hPa on (b) 2 February 1200 UT and (c) 3 February 1800 UT, corresponding to the respective central PSC levels. Color-coded temperatures range from 180 to 240 K. The vortex edge at 450 K is outlined by the 34 potential vorticity units (PVU) contour for 31 January. White lines in Figure 2a indicate the positions of the observed layers from 31 January, 2 and 3 February tracked back to 31 January, based on particle backward trajectories. Lower panels: Horizontal wind (arrows) and vertical wind (color-coded) from ECMWF analyses on (d) 31 January 1200 UT, (e) 2 February 1200 UT and (f) 3 February 1800 UT. The length of the arrows is proportional to the wind speed, whereby the longest arrows correspond to wind speeds of 6 m/s, 4.5 m/s and 2.5 m/s on 31 January, 2 and 3 February, respectively. Blue lines indicate the flight paths. The domain ranges from 68°N to 80°N and from 0°E to 30°E. See color version of this figure at back of this issue.

particle parameters. With the aid of precise meteorological analyses, w_p can be derived from successive lidar observations of selected PSC layers. Under the conditions of the measurements (about 80 hPa and 194 K) the sedimentation velocity of spherical particles of a few micrometers radius grows approximately quadratically with the particle radius. Additionally considering the Cunningham correction leads to increasingly enhanced falling velocities for particles smaller than the mean free path of air molecules. The gravitational sedimentation velocities of particles with different sizes are listed in Table 1. Cylindric particles experience slightly lower settling velocities as compared to spherical ones. Sedimenting ice particles are slower by an approximate factor of 0.7 due to their lower density [*Müller and Peter*, 1992; *Pruppacher and Klett*, 1997].

[8] The observation of the particles' sedimentation relative to the air mass they are embedded in of course must consider the vertical movement of the air itself. Actually, vertical winds can be taken from ECMWF analyses but it cannot be excluded that their inaccuracy is of the order of a significant fraction of the effect in question. The maybe largest uncertainties arise from the contribution of subsynoptic-scale atmospheric waves (e.g., induced by frontal systems). Their position and strength, however, changes daily and, if not represented in the analysis, would result

Table 1. Gravitational Sedimentation Velocity of Nitric Acid Trihydrate (NAT) Particles, Taking the Cunningham Correction Into Account[a]

Radius, m ($\times 10^{-6}$)	u-Stokes, m/h	u-Sphere, m/h	u-Cylinder, m/h
3	9.1	12.3	9.66
4	16.2	20.5	16.5
5	25.4	30.7	25.1
6	36.5	42.9	35.6
7	49.7	57.2	47.9
8	65.0	73.5	62.0
9	82.3	91.9	77.9
10	101.6	112.3	95.6
11	122.9	134.7	115.2
15	134.4	146.6	125.7

[a] Here, ρ = 1.6 g/cm^3. The numbers are valid for 80 hPa and 194 K.

in different sedimentation velocities on different days. Additionally, air mass trajectories indicate the temporal development and thus their consideration may improve the reliability of the vertical winds, although they also depend on the data quality in the Ice Sea region.

[9] The sedimentation velocity of the PSC particles is derived by a statistical approach, which is based on 2-D backscatter sections along colocated outgoing and incoming flights. The images reveal a vertical shift of individual PSC layers between the two successive measurements. The alignment of the flights ensures that nearly the same details of selected PSCs were underflown twice within 1 to 2 hours. The most precise results can be achieved from quasi-Lagrangian flights (i.e., parallel to the wind at PSC level), since in this case the same PSC structures were observed with some horizontal translation along the path, only. One also could try to catch selected structures twice by translating the second flight leg corresponding to the PSC-level wind. In order to fly as far as possible into the cold vortex regions, however, we chose straight flight patterns perpendicular to the vortex edge. In this case the horizontal advection across the flight paths introduces uncertainties depending on small-scale inhomogeneity and a possible isobaric slope of the layers as the lidar altitudes are based on pressure. In each of the 2-D along-flight backscatter sections, a highly detailed atmospheric structure is revealed by a contrast in the backscatter ratio. This contrast is primarily due to the spatial variability of the particle concentration. Particularly, since the coherent patterns in the backscatter ratio are contaminated by uncorrelated instrumental noise, a statistical technique has the very attractive property of simultaneously retrieving/correlating structures on a variety of spatial scales and over a large measured range. The implicit focus on larger scales minimizes the influence of noise on the boundary retrieval and identifies even small shifts of subtle but coherent structures.

[10] For the determination of the vertical shift of the PSC layers between two successive flight legs, a cross-covariance analysis using the 2-D backscatter ratio sections is applied. The analysis refers to identical latitude-altitude ranges where the structures are observed clearest. The resulting lagged cross-covariance function, represented by a matrix of covariances cov (x_j, x_k) contains the covariance as a function of the horizontal (x_j) and vertical (x_k) displacement of the 2-D backscatter sections. The position of the absolute maximum of the matrix cov (x_j, x_k) corresponds to the number of range bins by which the layers, measured twice within a few hours, are spatially shifted against each other. The covariance elements $\mu_{j,k}$ of cov (x_j, x_k) are calculated by step 1, fast Fourier transformation (FFT) of the 2-D backscatter ratio arrays to the spectral space, followed by step 2, the Fourier-back-transformation of the product of the spectral representation of array 1 (northward leg) and the complex conjugate of array 2 (southward leg). The correlation coefficient can then be calculated from cov (x_j, x_k) via r = cov (x_j, x_k)/($\sigma_j * \sigma_k$), σ_j and σ_k being the standard deviations of the backscatter ratio arrays in the horizontal and the vertical. A geometrical vagueness results from correlating two spatially (and temporarily) extended cloud sections, since the sedimentation distance increases linearly from the beginning to the end of the compared sections. This vagueness could be minimized by "bending" the second section according to the sedimentation velocity resulting from an a priori analysis. However, to exclude bad data, we correlate only relatively short sections, for which this vagueness quantitatively corresponds to the resolution of the lidar data (30 m vertically) and therefore cannot be eliminated satisfactorily. Another prerequisite for this analysis is that the compared PSC structures are largely stationary for more than the 1–2 hours between the pairs of measurements. The observed persistence of the pronounced layers over at least 4 days indicates that the timescales of dynamical developments are indeed large compared to the duration of the missions.

3. Results

3.1. Geometrical Structure

[11] Vertical sections of the backscatter ratio into the vortex core are shown in Figures 3–5 from the missions on 31 January, 2 and 3 February 2000. On all flights, stacked synoptic-scale PSCs with pronounced particle layers were observed in the lower stratosphere where temperatures were below T_{NAT}. The vertical depth of the layers was about a few hundred meters. Near their southernmost edge they reach up to an altitude of about 19 km on 31 January (72°N, 15°E), to ≈17 km on 2 February (72°N, 15°E) and only 16 km on 3 February (70°N, 20°E). In the southern section of the flight legs the layers turn into a diffuse aerosol layer covering approximately the same altitude range. The PSC base is evident on 31 January while on 2 February the backscatter ratio gradually decreases below the main cloud and reaches down to the extraordinarily high tropopause/hygropause indicated by cirrus clouds at 11 km altitude. On 3 February, the PSC base erroneously seems to occur near 13.5 km; however, this is an instrumental artifact due to optical misalignment that affects the received signal below this altitude. The boundary of the PSC layers approximately matches the NAT temperature threshold T_{NAT}. The weakly backscattering aerosol layer is known as Junge layer and according to its optical properties presumably consists of volcanic emissions [e.g., *Jäger et al.*, 1995]. It reaches up to 20 km altitude and seems to coexist with the PSCs. The strongest recent volcanic sources were Shishaldin (Aleutian Islands, April 1999) and Gua Gau Pichincha (Equador, October 1999). At the

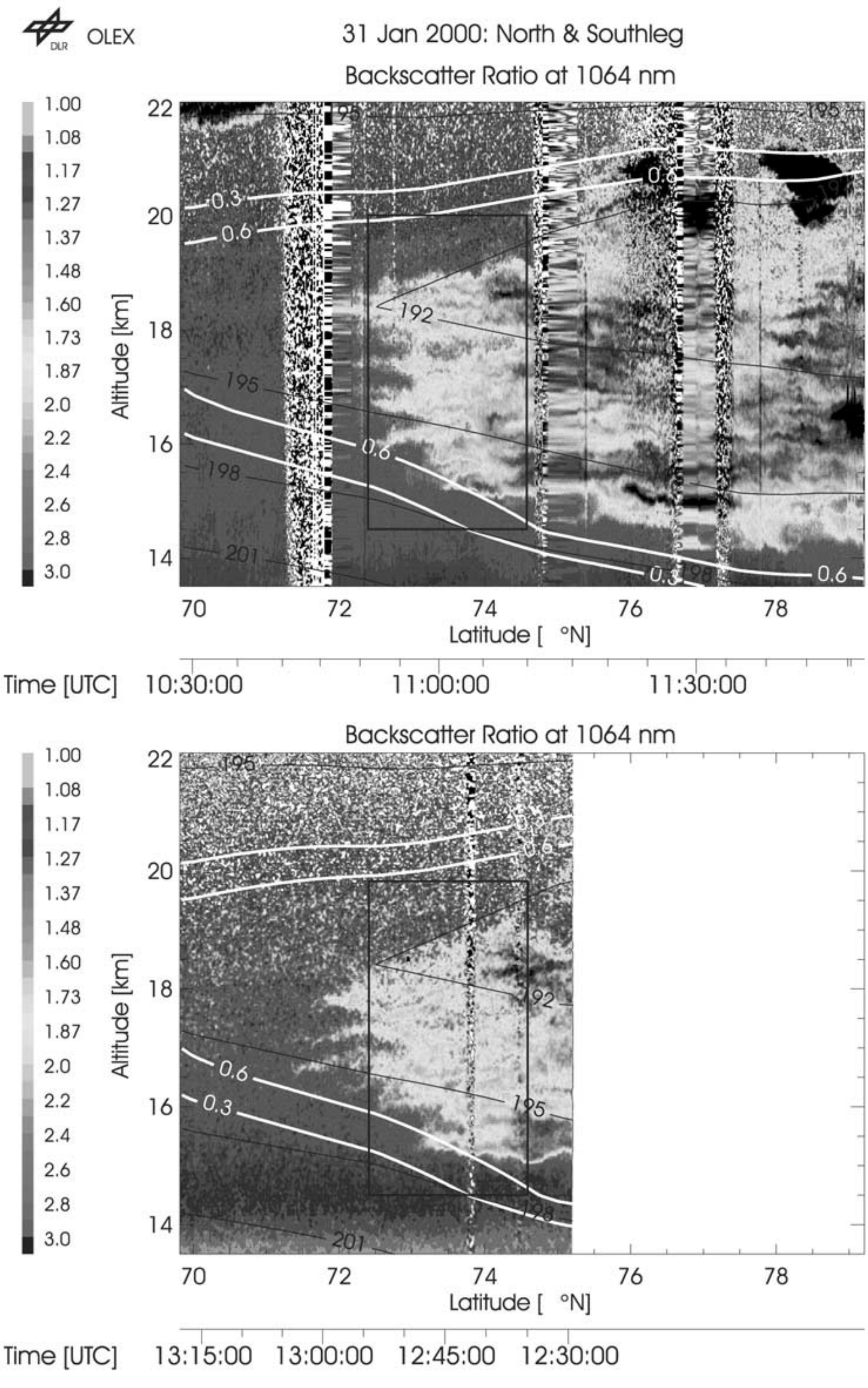

Figure 3. Backscatter ratio along the Falcon flight paths on 31 January 2000, not corrected for extinction, in order to maintain high spatial resolution. Each pair of panels shows the northward and southward legs of 2–3 hour turning point missions. Overlayed are contours of ECMWF temperature and of the fraction of HNO_3, which according to the phase diagram of *Hanson and Mauersberger* [1988] is in the (solid) NAT-phase, assuming 4.5 ppbv H_2O and a HNO_3 vertical column of 2.5×10^{20} m^{-2}. Noisy profiles result from strong extinction (shadowing) of the laser beam by cirrus clouds or are due to instrumental artifacts. The cloud section selected for the cross-covariance analysis is marked by a black frame. See color version of this figure at back of this issue.

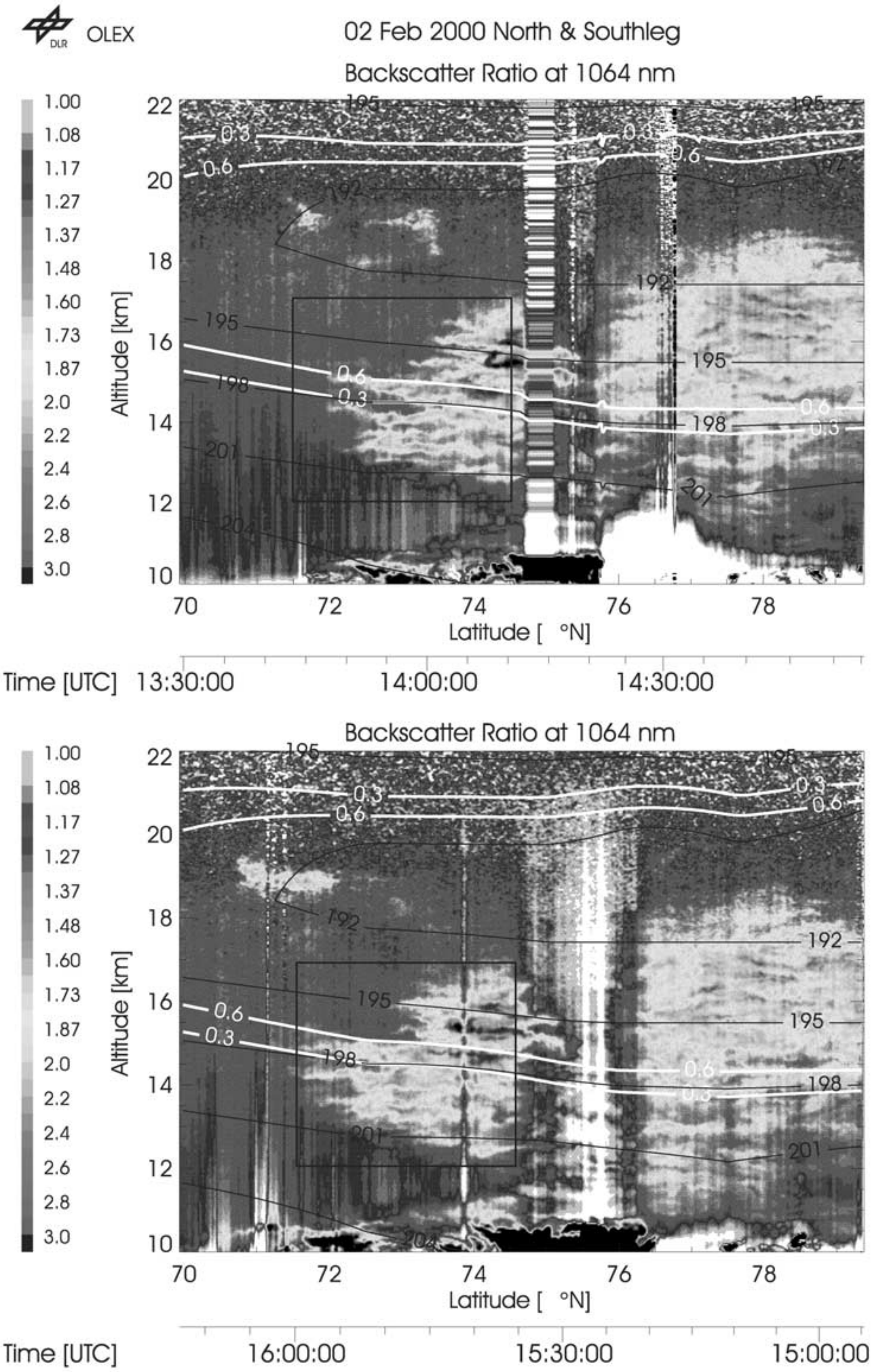

Figure 4. Backscatter ratio along the Falcon flight paths on 2 February as in Figure 3. The black (color-saturated) regions around 10.5 km altitude indicate strongly back-scattering cirrus clouds. In the PSC free region the volcanically produced BG-aerosol layer is evident below 20 km. The layers at that time already occurred at significantly lower altitudes than prescribed by the [NAT]/[HNO_3]-ratio isolines, which indicates denitrification at the upper levels and nitrification below (see text). See color version of this figure at back of this issue.

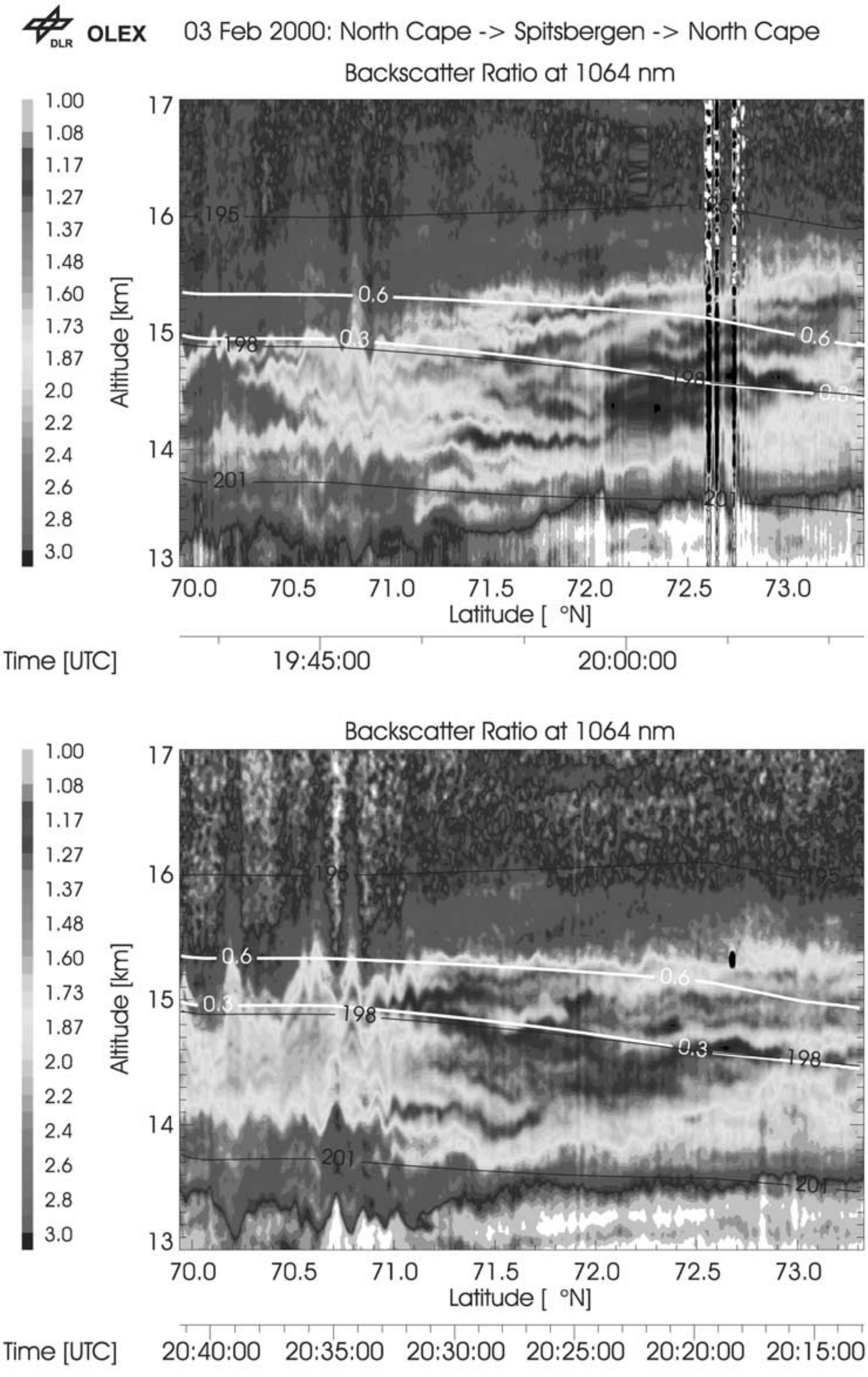

Figure 5. Backscatter ratio along the Falcon flight paths on 3 February as in Figure 3. The ER-2 contrail was observed at 2018 UTC near 72.7°N in 15.3 km. As compared to Figure 4 the denitrification/nitrification process had proceeded further. See color version of this figure at back of this issue.

frayed boundary of the PSCs single layers with enhanced backscatter ratio extend several 100 km into the warmer region. Dynamical structures like this can also be observed as ozone laminae and are typically generated by differential vertical shear that is not aligned with tracer surfaces and thus converts horizontal tracer gradients into vertical ones [*Appenzeller and Holton*, 1997]. Owing to the stable stratification these layers extend far into the vortex. Buoy-

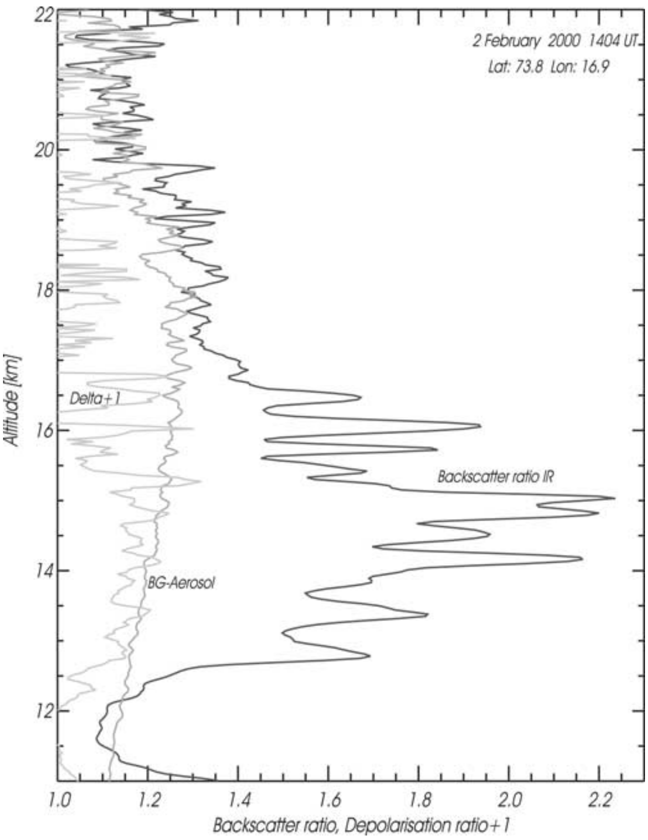

Figure 6. Profiles of total backscatter ratio γ_{1064} at 1064 nm (blue), background aerosol $\gamma_{BG,\ 1064}$ (red), particle depolarization ratio (corrected for contribution of background aerosol) δ_{532} at 532 nm (green) on 2 February 2000, 1404 UT. See color version of this figure at back of this issue.

ancy gravity waves occur above the North Cape ($\approx$71°N) on 3 February with scales of a few tens of kilometers. They are orographically forced and propagate upward to the stratosphere.

3.2. Optical Properties

[12] The background aerosol layer outside the cold vortex core can be distinguished from the NAT PSCs by strong backscatter gradients at the PSC edges and by the very low depolarization (not shown). The backscatter ratio in this layer reaches peak values of γ_{1064nm} = 1.25 around 18 km and drops to $\gamma_{1064nm} \approx 1.1$ above 20–21 km. In Figure 6 the BG-profile taken outside the PSCs at 70°N to 71°N on 2 February shows the BG-offset to the backscatter profile inside the PSC (73.8°N). It must be taken into account when the optical properties of the PSC particles are calculated. The BG-aerosol does not depolarize and most likely consists of volcanically produced liquid particles, which are known to be predominantly composed of sulfuric acid solution (H_2SO_4/H_2O) [*Turco et al.*, 1982; *Jäger et al.*, 1995]. Against this, moderate depolarization between 15 and 20% are observed in the PSC layers (green profile in Figure 6). Peak total backscatter ratios of the PSC layers are about γ_{1064nm} =2–3 (γ_{532nm} = 1.1) inside the cold vortex core and γ_{1064nm} = 1.8–2 near the PSC boundary. The corresponding particle backscatter ratios are $\gamma_{Aer} = \gamma_{total} - 1$. The ratio of the backscatter coefficients $\beta_{532nm}/\beta_{1064nm}$ (color ratio) ranges around 1–1.5 inside the PSCs, indicating large particles, and values much larger than 1 in the BG-aerosol indicating small particles compared to the laser wavelength. According to T-matrix calculations [*Mishchenko*, 1991; *Carslaw et al.*, 1998; *Wirth et al.*, 1999] for axially-symmetric stratospheric particles of different compositions, the observed synoptic PSC layers ($\gamma_{1064nm} = 1.8 - 2$, $\delta_{532nm} = 0.15 - 0.2$) are most likely composed of prolate (aspect ratio $\approx$0.6–0.9; compare Figure 7b) nitric acid trihydrate (NAT) particles with effective radii larger than 2–3 μm (Figure 7). Owing to the spectrally limited lidar wavelength range the information content with respect to large particle sizes is limited, correspondingly. In situ measurements on board the NASA ER-2 aircraft even indicate radii up to 10 μm for these particles. This extraordinarily large size lead to the designation as "NAT-rocks" [*Fahey et al.*, 2001; S. D. Brooks et al., manuscript in preparation, 2002; B. Luo, et al., Large stratospheric particles observed by lidar during SOLVE/

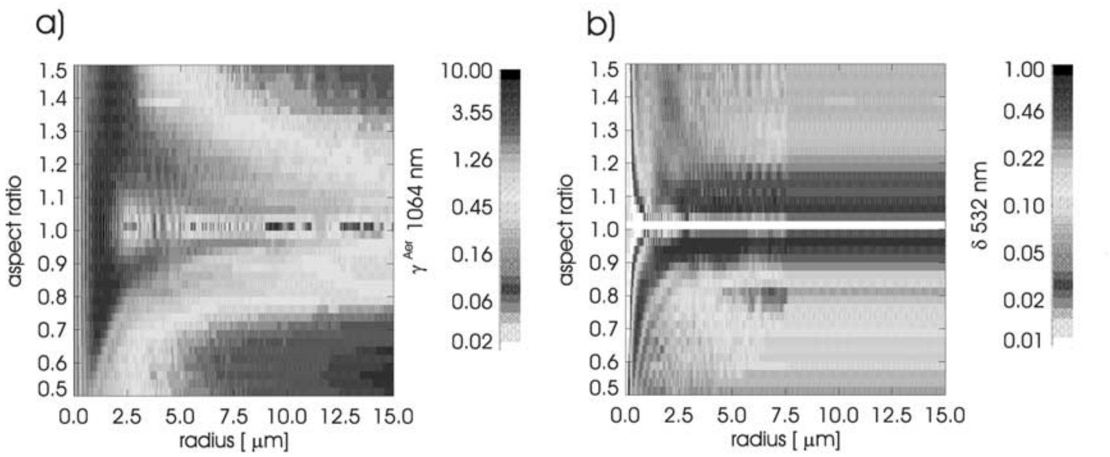

Figure 7. T-matrix calculations for spheroidal NAT particles with 1 ppbv condensed HNO_3: (a) Backscatter ratio at 1064 nm, (b) depolarization ratio at 532 nm. The backscatter ratio is proportional to the NAT particle mixing ratio. The particles are assumed to be lognormally distributed with a mode width of σ = 1.2. See color version of this figure at back of this issue.

THESEO2000 mission, submitted to *Journal of Geophysical Research*, 2001] (hereinafter referred to as Luo et al., submitted manuscript, 2001). Particles of several microns radius settle considerably by gravitation on timescales of hours to days. The vertical separation of the layers, which persisted for several days, indicates that the particle size distribution must have been nearly monodisperse. The observed layering in the backscatter ratio thus is most likely caused by different particle concentrations rather then by optically differently effective sizes and phases. Otherwise their different sedimentation velocity, which is a strong function of the radius in this size range, would have mixed the layers vertically within about 1 day. Only a continuous gradient- stabilization or -generation mechanism could maintain the layering in the presence of a pronounced polydisperse particle size distribution. The nature of such a mechanism, however, would have to be too selective over a large horizontal and vertical range to appear likely.

[13] Overlayed to the color-coded backscatter sections in Figures 3–5 are isolines of ECMWF temperature and of the fraction of HNO_3, which according to the phase diagram of [*Hanson and Mauersberger*, 1988] is in the (solid) NAT-phase. The NAT-fraction is calculated from ECMWF temperatures assuming a water vapor mixing ratio of 4.5 ppmv [*Schiller et al.*, 2002] and a HNO_3 column of $2.5 \times 10^{20} m^{-2}$ which is a standard value for recent years. Owing to the constant H_2O and HNO_3 values, the NAT isolines essentially follow the large-scale NAT threshold temperature in the sense that NAT particles may, but need not necessarily, form when an air mass is cooled below T_{NAT} (which would be the zero isoline just outside the [NAT]/[HNO_3] = 0.3 contour). It indicates how close the observed NAT PSCs are to thermodynamical equilibrium and provides an indication of the age of the particles. According to Figures 4 and 5, denitrification is evident at the upper levels and nitrification below: Nitrification by falling and evaporating NAT particles increases the HNO_3 mixing ratio in the lowermost stratosphere (up to 13 ppbv in the 1999–2000 winter) so that the profiles deviate considerably from the mean standard profile of Arctic winters. Therefore the determination of T_{NAT} in those regions critically depends on the amount of evaporating NAT particles (nitrification) and is subject to large uncertainty. Thus, on 2 and 3 February NAT-layers at lower altitudes were also observed in the lowermost stratosphere a the low side of the isolines of the [NAT]/[HNO_3] ratio. This most likely is due to nitrification-enhanced HNO_3 vapor pressure as compared to the assumed standard profile but may partly also be attributed to the delayed evaporation of the falling particles, which can survive nearly 1 day at 1 K above T_{NAT} (and meanwhile sediment about one km).

[14] As described in section 2, the very narrow particle size distribution allows to determine the particle sizes via their viscous-friction-decelerated sedimentation, which is a strong function of the particle's sizes and density and a weak function of their shapes. It is evident from visual inspection of the backscatter sections that the PSC layers as a whole occur at significantly lower altitudes each other day. Since Figure 2a shows that the observed PSC sections on 31 January are close to each other, this confirms that a settlement occurs on large scales. As stratospheric temperatures in the Ice Sea region gradually decreased during the period, it took at least several days for the particles to grow to such large sizes. Besides the intraday settlement, a significant sinking of the layers by 100–200 m is evident even between the outgoing and the incoming flight legs from single missions. Simultaneously, the vertical velocity of the air mass as analyzed by the ECMWF was nearly negligible.

3.2.1. Observations on 31 January

[15] On 31 January 2000 NAT PSCs were observed north of 72°N where synoptic temperatures were well below the NAT threshold (compare Figure 3). The flight extended from 70°N to nearly 80°N, but only the section between 72°N and 75°N was probed twice by the lidar with time shifts of 2h 10min and 1h 20min at the southern and the northern points, respectively (Figures 3a and 3b). With a wind speed of 4 m/s at central PSC level (70 hPa) perpendicular to the flight direction, this time shift corresponds to about 20 km spatial shift between the observations on the outgoing and the incoming flight legs. The layering was most pronounced at the cloud's edge but was evident over the entire section. Owing to several bad profiles, only the southern part of the PSC is selected for the analysis. The vertical wind inside the observed PSC section (65–120 hPa) as analyzed for 1200 UT by the ECMWF ranges from $w \approx -0.2$ cm/s at 120 hPa, 74°N to $w \approx -1.0$ cm/s at 65 hPa, 72.4°N. It contributes about 37 m to the observed particle settling. In Figure 3 the isolines for the NAT fraction [NAT]/[HNO_3] = 0.3 and 0.6 follow the outer bounds of the NAT layers except at their southern edge. Though NAT particles would have also been stable south of the observed PSCs, the low backscatter and depolarization ratios indicate that there was only BG-aerosol.

3.2.2. Observations on 2 February

[16] During the second mission on 2 February 2000, the NAT PSCs showed more pronounced layering (evident up to the turning point at nearly 80°N) and occurred at lower altitudes than during the previous measurement. While at their boundary their top was around 15 km, inside the cold vortex region they extended from the tropopause (or hygropause, indicated by cirrus clouds) up to 19 km altitude. Meanwhile the BG-aerosol had not changed significantly. Also the layers' optical properties were the same as observed 2 days before (Figures 4a and 4b). During the 2 hours between the first and the second observations the frayed boundary of the NAT-PSC propagated southward from 72°N to 71.5°N. At the southernmost point where the layers were most pronounced, they were confined to the 13–15 km altitude range. According to the correlation analysis the settling of the layers at their southern edge amounted to $\Delta h = -130$ m within the 1.85 hours between the measurements. The selected PSC region is outlined by a black frame in Figure 4. The temperature profile stays close to T_{NAT} over the height range of the layers. Correspondingly, the particle sedimentation velocity $w_p \approx 70$ m/h does not differ significantly between the base and the top of the PSC. According to ECMWF analyses the vertical wind was close to zero over the vertical range of the PSC near 72°N to 74°N and therefore is negligible for our considerations. Also, the settling of the layers relative to the BG-aerosol confirms that the observed sedimentation of the particles is not due to large-scale subsidence of the air mass in which

they are embedded. The layers are slightly sloping meridionally and roughly follow the ECMWF isotherms over a distance of nearly 1000 km from 70°N to 79.7°N.

3.2.3. Observations on 3 February

[17] On 3 February 2000, only a relatively short section between the North Cape and the Bear Island (74.5°N, 20°E) was flown below the NAT layers. This time, backscatter signals of NAT particles like on the days before were measured only below 15.5 km altitude (Figures 5a and 5b). The PSC base occurred below 13 km but cannot accurately be determined since the optical system was slightly misalignment. The layers on this day were undulated by orographically induced gravity waves on different scales and with vertical amplitudes of several 100 m. Though the flight was nearly quasi-Lagrangian, the waves, combined with strong horizontal wind, and the fact that only relatively short sections with small time shift were measured, makes this case inappropriate for the correlation analysis. Nevertheless, together with the other observations, it demonstrates the enormous extension of the NAT layers over the European Ice Sea during the 4-day period since 31 January 2000.

4. Discussion

[18] A rough classification of the observed PSC layers' backscatter and depolarization ratios according to the empirical scheme of *Browell et al.* [1990] and *Toon et al.* [1990] reveals that they can be assigned to type Ia (low backscatter ratios, moderate depolarization). Early lidar observations of such PSCs lead to the hypothesis that they are most likely composed of nitric acid trihydrate (NAT) particles [*Crutzen and Arnold*, 1986; *Hanson and Mauersberger*, 1988; *Toon et al.*, 1986]. Persistent cold temperatures in the Arctic vortex during December 1999 and January 2000 around or just below the NAT equilibrium allowed the formation of very large particles. Meanwhile, the occurrence of NAT has been confirmed in mountain wave induced Ia-enhanced PSCs by balloonborne massspectrometer analyses of PSC particles [*Schreiner et al.*, 1999; *Voigt et al.*, 2000]. The empirical interpretation as NAT particles is confirmed by T-matrix analyses of the optical properties of the layers observed over the Northern European Ice Sea. It indicates that the layers consisted of unspherical prolate NAT particles with radii larger than $r_p = 2-3$ μm and an aspect ratio of 0.6–0.9. The results also agree with airborne lidar data from the NASA DC-8 (Luo et al., submitted manuscript, 2001) and with in situ NO_y and MASP measurements [*Fahey et al.*, 2001; S. D. Brooks et al., manuscript in preparation, 2002] on board the NASA ER-2. The NO_y instrument of fahe.01 employed forward and backward pointing inlets allowing them to sample gas phase and particulate NO_y, simultaneously. It discovered very large particles with $r_p = 3 - 10$ μm. The backscatter, color and depolarization ratios of the layers do not change significantly within the 3 days indicating thermodynamical and chemical passivity. Owing to the spectrally limited information content of the lidar data only a lower limit for the particle size can be derived by means of the T-matrix analysis but the precise radius can be determined from the sedimentation velocity of the observed particles. Therefore we compared the altitudes of their backscatter signatures at two successive times, which is objective and capable to take all the information of extended sections of the layers into account. The cross-covariance analysis of the vertical positions of the NAT layers yields their downward movement with high accuracy whereby it is crucial to show that the NAT particles indeed settle relative to the surrounding air with a velocity determined by their size, shape and composition. The latter parameters must be taken from the T-matrix analyses. Strong arguments for the sedimentation are the negligible or well known synoptic-scale vertical wind analyzed by the ECMWF and the constant altitude of the small BG-aerosol particles in the vicinity of the NAT layers.

[19] The most robust results are obtained from the measurement on 2 February since this mission in good approximation was quasi-Lagrangian both outgoing and incoming. The ECMWF analyzed vertical wind at that time was close to zero in the relevant region. In addition, the pronounced separation of the individual layers enhances the sensitivity of correlating the layers' internal structure at different times. As displayed in Figure 8a the correlation of the backscatter sections reaches a maximum, i.e., the overlap of the selected cloud regions is best, for a relative shift of several km horizontally and −130 m vertically. The cloud region selected for the covariance analysis (71.5°N to 74.6°N, 12–17 km altitude) is outlined in Figures 4a and 4b. The calculated horizontal shift has no relevance, since the observed structures are horizontally too homogeneous and are partly autocorrelated on scales smaller than the wind shift. In the vertical, the layers produce significant correlation maxima as a function of the vertical lag between both images. Actually, in addition to the main maximum at −130 m a side maximum occurs at −700 m which reflects the mean vertical distance between the layers and results from skipping one layer-distance matching the next but one layers. The ECMWF- analyzed w-wind in the selected cloud region was -0.2 cm/s $< w <$ 0.2 cm/s ($\approx$7 m/h) and only adds an uncertainty (Figure 2e). The uncertainty of the ECMWF analyses is estimated to be about an order of magnitude less than the observed sedimentation. Since the altitude of the volcanic aerosol layer can not be determined with the required accuracy (small gradients) and the cirrus clouds below the NAT layers (with particles of unknown size) are also subject to both sedimentation and vertical air motion, these observations cannot be used to support this analysis. The resulting sedimentation velocity thus amounts to $w_{p,sedi} \approx -70 \pm 8$ m/h, referred to the southerly edge (73°N) of the PSC layers.

[20] Roughly the same sedimentation velocity can be derived from the measurement on 31 January, though in this case the wind direction was nearly perpendicular to the flight path introducing approximately 25 km horizontal shift between the compared cloud sections. In spite of this, the structures near the PSCs' edge are very similar in both sections and indicate sufficient along-stream homogeneity on the relevant scales. The cloud region from 72.4°N to 73.7°N and 14.5 to 20 km altitude was selected for the covariance analysis. As shown in Figure 8b the analysis yields a downward movement of the layers by about 160 m within 1h 45 min. Taking into account that the vertical wind as analyzed by the ECMWF was about $w \approx -0.6$ cm/s (≈ -22 m/h) we get a sedimentation velocity of about $w_{p,sedi} \approx -69 \pm 3$ m/h at 73°N, about the same as on 2 February. The estimated uncertainty in the observed settlement velocity of

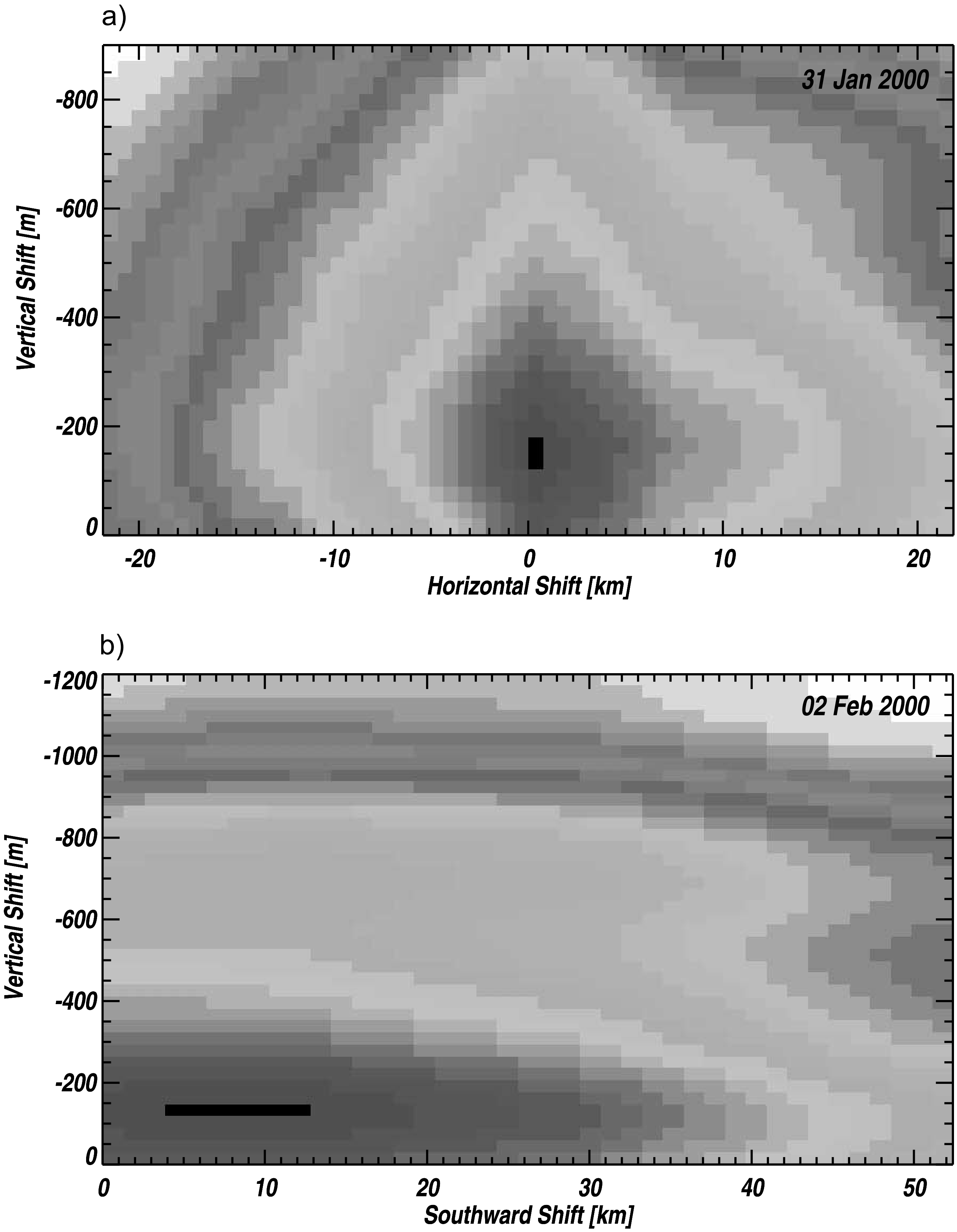

Figure 8. Covariance matrices for the horizontal and vertical shifts of selected backscatter ratio regions of the NAT layer PSCs on 31 January (a) and 2 February (b). The latitude/altitude sections cut for the analysis are [72.4°N to 73.7°N, 14.5–20 km] and [71.5°N to 74.6°N, 12–17 km] for 31 January and 2 February, respectively (compare Figures 3 and 4). Covariances are linearly rainbow color-coded in arbitrary units. The local maxima appear in black and indicate the shifts required for a best match of the selected data arrays. See color version of this figure at back of this issue.

the particles as provided by the covariance analysis amounts to approximately 3 m/h. The error of the ECMWF analyses was estimated to be $\Delta w \approx \pm 0.2$ cm/s or $\Delta w \approx \pm 7$ m/h, based on the horizontal and vertical variability. The layers' altitudes were calculated from pressure and the signal runtime times speed of light. The error for this is negligible as the ECMWF pressure near 100 hPa varied by less than 0.1 hPa ($\equiv$ 5 m) during the mission. With these contributions, the uncertainty of the derived sedimentation velocity is about $\delta v_{sedi} \approx 12$ m/h, so considering both days we end up with a sedimentation velocity of the NAT particles of $w_{p,sedi} = -69 \pm 14$ m/h. Referring to Table 1, this corresponds to a particle radius $r_{NAT} \approx 8 \pm 1$ μm. The results from 3 February is not appropriate for this analysis but confirms the enormous extension of the NAT layers over large regions of the vortex core.

4.1. Downward NO_y Flux

[21] Proposing that the PSC layers consisted of 8 μm NAT particles, the T-matrix calculations (Figure 7) can be used to derive an estimation for the mixing ratio of condensed HNO_3 which again is assumed to be completely incorporated in the NAT particles. The calculations shown in Figure 7 are based on a condensed HNO_3 concentration of 1 ppbv and a lognormal size distribution ($\sigma_{radius} = 1.2$). Excluding the existence of other particles, the calculated backscatter ratio is simply proportional to the condensed particle mixing ratio. According to Figure 7, 1 ppbv of 8 μm NAT particles with an aspect ratio of 0.6–0.9 (compare section 3.2) yield particle backscatter ratios between $0.3 < \gamma_{Aer,1064nm} < 1$. A backscatter ratio of $\gamma_{Aer,1064nm} = 0.8–1$ ($\gamma_{total,1064nm} = 1.8–2$ in Figures 3–5) observed in the PSC regions taken for the analysis thus corresponds to 1–3 ppbv of NAT. (Note that Figure 7 refers to the particle backscatter ratio γ_{Aer} while Figures 3–5 show the total backscatter ratio $\gamma_{total} = \gamma_{Aer} + 1$.) With a molecular weight of 117 u (unified atomic mass units), a density of 1.6 g cm^{-3} and a particle radius of 8 ± 1 μm, each NAT particle contains $18 \pm 8 \times 10^{12}$ molecules. At 70 hPa, 1–3 ppbv correspond to concentrations of $2 - 6 \times 10^9$ molecules/cm^3. The NAT particle concentration then varies between $[NAT]_{part} \approx 1 \pm 2 \times 10^{-4}$ cm^{-3} and $[NAT]_{part} \approx 3 \pm 2 \times 10^{-4}$ cm^{-3} in the thinner and denser PSC regions. If particulate NO_y had completely condensed into NAT, the downward NO_y-flux is given by the NAT-flux $d[\mathrm{NAT}]_{mix}dz/dt \approx 3.3 \pm 1.6$ ppbv km/d.

4.2. Denitrification Potential

[22] The optical properties and the internal structure of the "NAT rock" PSCs did not change significantly within the 4 day period in which they were observed. This either means that we stayed in the plume or generally the impact area of a persistent localized generation mechanism (e.g., mountain waves over Greenland) or that the lifetime of the layered PSCs was at least of the order of a week and they extended over a correspondingly large area. From particle backward trajectories we conclude that we most likely repeatedly probed different parts of essentially the same widespread cluster of particle layers, distributed homogeneously over large parts of the Arctic vortex. The observed particles were tracked back to different vortex regions by ECMWF air mass trajectories to which we assigned sedimentation rates that produce 8 μm particles at the observed times and locations. The distribution/extension of the probed volumes over the vortex provides an indication of how representative these observations are for the early February 2000 Arctic vortex. The white lines in Figure 2a indicate the positions from where the particles, observed during the three missions, were transported since 31 January, based on ECMWF particle back trajectories. The particles measured on 2 February remained below the NAT equilibrium since 31 January and thus most likely existed without intermittency along their trajectories. The widespread extension of this cloud type is supported by lidar measurements with the NASA Langley/NASA Goddard instruments few days before on board the NASA DC-8 [*Hostetler et al.*, 2000; *Browell et al.*, 2000]. The agreement of the NAT-layers' extension with the region in which most HNO_3 exists as NAT (white lines in Figures 3–5) indicates that the layers were still close to thermodynamical equilibrium on 31 January. During the following days the layers seemed to fall out of the region enclosed by the 60% NAT-fraction isoline. This indicates that the observed particles were already aged and no significant particle transformation processes took place; i.e., these particles, except from their sedimentation, were passively advected. Therefore, we conclude that a considerable fraction of the European vortex was covered by the sedimenting NAT particle layers. Along with the large-scale dehydration observed by *Schiller et al.* [2002], the large area subject to the downward HNO_3-flux derived above, indicates that the observed NAT layers had the potential to contribute crucially to the denitrification observed in the Arctic stratosphere in the winter 1999–2000.

5. Conclusions

[23] We have shown airborne lidar measurements of extended particle layers inside the cold vortex core south of Spitsbergen in the 1999–2000 winter. Three missions were performed over the European Ice Sea in late January to early February 2000, with colocated outbound and inbound flight legs. Single layers are evident at significantly different altitudes in the pairs of backscatter sections. We conclude that this settlement must be interpreted as a gravitational sedimentation of the particles owing to their large sizes. The pronounced and persistent vertical structure of the layers indicates that the particle size distribution must have been very narrow, because otherwise different sedimentation velocities (in the absence of an active layer-generating mechanism) would have quickly eliminated the vertical gradients. This again implies that the observed inhomogeneities are due to differences in the particles' concentrations rather than their optical efficiency. The microphysical analyses based on empirical classification and on T-matrix calculations indicate that the layers were composed of large nitric acid trihydrate (NAT) particles with radii $r_p > 2 - 3$ μm. Based on cross-covariance analyses of extended along-flight-path sections of the particle backscatter ratio measured during outgoing and incoming flights, we derive a sedimentation velocity of $w_{p,sedi} \approx 69 \pm 14$ m/h corresponding to particle sizes of about $r_p \approx 8 \pm 1$ μm. With about 1–3 ppbv of condensed HNO_3 the downward NO_y-flux (given by the NAT-flux) is $d[NAT]_{mix}dz/dt = 3.3 \pm 1.6$ ppbv km/d.

Based on ECMWF particle back trajectories we deduce that a large fraction of the vortex area was subject to denitrification by the sedimenting large NAT particles.

[24] Synoptic-scale polar stratospheric clouds (PSCs) have been measured with an aircraft-borne lidar south of Spitsbergen in early February 2000. The PSCs of moderately depolarizing stratified layers extended from near the tropopause (10–11 km) up to 20 km altitude. Their internal structure in backscatter ratio reflects the variability of the particles' concentration rather than manifold sizes and phases of different optical efficiency. Actually, their size distribution was nearly monodisperse. According to T-matrix calculations, low backscatter ratios ($\gamma < 3$), color ratios of 1–1.5 and moderate depolarization ratios ($\delta_a \approx 0.15–0.2$) indicate that the observed layers were composed of aspherical NAT particles larger than 2 μm. During three turning point missions into the cold vortex core a significant settling of the particle layers was observed between aligned outgoing and incoming legs. Low stratospheric winds and quasi-Lagrangian flight heading minimized horizontal drifts between the probed volumes. A NAT particle sedimentation velocity of 69 $\pm$ 14 m/h is derived by cross-covariance analysis of corresponding pairs of 2-D backscatter sections of the layers. This implies a particle size of $r_p \approx 7–8$ μm and a mixing ratio of condensed HNO_3 near 2 ppbv. The downward NO_y flux below 19 km altitude amounts to $j \approx 3$ ppbv km/d. Based on particle back trajectory analysis, this flux, derived from the observations in different regions of the Northern European Ice Sea, has a significant denitrification potential.

[25] **Acknowledgments.** We are grateful to Heini Wernli from ETH Zürich, who wrote the code for extracting the synoptic parameters to prescribed pressure or theta levels and supported its implementation. We acknowledge the European Centre for Medium Range Weather Forecasts (ECMWF) for providing high-quality analysis data. The study was supported by the European Community within the fifth framework project THESEO 2000.

References

Appenzeller, C., and J. R. Holton, Tracer lamination in the stratosphere: A global climatology, *J. Geophys. Res.*, *102*, 13,555–13,569, 1997.

Browell, E. V., C. F. Butler, S. Ismail, P. A. Robinette, A. F. Carter, N. S. Higdon, O. B. Toon, M. R. Schoeberl, and A. F. Tuck, Airborne lidar observations in the wintertime Acrtic stratosphere: Polar stratospheric clouds, *Geophys. Res. Lett.*, *17*, 385–388, 1990.

Browell, E. V., C. F. Butler, W. B. Grant, V. G. Brackett, S. A. Kooi, O. B. Toon, J. Burris, T. McGee, M. Schoeberl, and M. J. Mahoney, Polar stratospheric cloud characteristics observed during the SOLVE campaign, paper presented at THESEO2000/SOLVE Workshop, Eur. Comm., Palermo, Italy, Sept. 2000.

Carslaw, K. S., M. Wirth, A. Tsias, B. P. Lou, A. Dörnbrack, M. Leutbecher, H. Volkert, W. Renger, J. T. Bacmeister, and T. Peter, Particle microphysics and chemistry in remotely observed mountain polar stratospheric clouds, *J. Geophys. Res.*, *103*, 5785–5796, 1998.

Crutzen, P., and F. Arnold, Nitric acid cloud formation in the cold Antarctic stratosphere: A major cause for the springtime ozone hole, *Nature*, *324*, 651–655, 1986.

Dörnbrack, A., T. Birner, A. Fix, H. Flentje, A. Meister, H. Schmid, E. V. Browell, and M. J. Mahoney, Evidence for inertia-gravity waves forming polar stratospheric clouds over Scandinavia, *J. Geophys. Res.*, *107*, 10.1029/2001JD000452, in press, 2002.

Fahey, D. W., K. K. Kelly, A. F. Tuck, M. Loewenstein, K. R. Chan, and L. E. Heidt, Observations of denitrification and dehydration in the winter polar stratosphere, *Nature*, *344*, 321–324, 1990.

Fahey, D. W., et al., The detection of large HNO_3 particles in the winter Arctic stratosphere, *Science*, *291*, 1026–1031, 2001.

Flentje, H., W. Renger, M. Wirth, and W. A. Lahoz, Validation of contour advection simulations with airborne lidar measurements of filaments during the Second European Stratospheric Arctic and Mid-Latitude Experiment (SESAME), *J. Geophys. Res.*, *105*, 15,417–15,437, 2000.

Hanson, D. R., and K. Mauersberger, Laboratory studies of the nitric acid trihydrate: Implications for the south polar stratosphere, *Geophys. Res. Lett.*, *15*, 855–858, 1988.

Hintsa, E., et al., Dehydration and denitrification in the Arctic polar vortex during the 1995–1996 winter, *Geophys. Res. Lett.*, *25*, 501–504, 1998.

Hostetler, C., P. L. Lucker, M. T. Osborn, J. Burris, and T. McGee, Observation of PSCs and stratospheric aerosols from the LaRC aerosol lidar, paper presented at THESEO2000/SOLVE Workshop, Eur. Comm., Palermo, Italy, Sept. 2000.

Hübler, G., et al., Redistribution of reactive odd nitrogen in the lower Arctic stratosphere, *Geophys. Res. Lett.*, *17*, 453–456, 1990.

Jäger, H., O. Uchino, T. Nagai, T. Fujimoto, V. Freudenthaler, and F. Homburg, Ground-based remote sensing of the dacay of the Pinatubo eruption cloud at three Northern Hemisphere sites, *Geophys. Res. Lett.*, *22*, 607–610, 1995.

Kawa, S. R., et al., The Arctic polar stratospheric cloud aerosol: Aircraft measurements of reactive nitrogen, total water and particles, *J. Geophys. Res.*, *97*, 7925–7938, 1992.

Kelly, K. K., et al., Dehydration in the lower Antarctic stratosphere during late winter and early spring 1987, *J. Geophys. Res.*, *94*, 11,317–11,357, 1989.

Kelly, K. K., et al., A comparison of ER-2 measurements of stratospheric water vapour between the 1987 Antarctic and 1989 Arctic missions, *Geophys. Res. Lett.*, *17*, 465–468, 1990.

Klett, J. D., Lidar inversion with variable backscatter/extinction ratios, *J. Appl. Opt.*, *24*, 1638–1643, 1985.

Kondo, Y., H. Irie, M. Koike, and G. E. Bodecker, Denitrification and nitrification in the Arctic stratosphere during the winter of 1996–1997, *Geophys. Res. Lett.*, *27*, 337–341, 2000.

Macke, A., M. I. Mishchenko, K. Muinonen, and B. E. Carlson, Scattering of light by large nonspherical particles: Approximation versus T-matrix method, *Opt. Lett.*, *20*, 1934–1936, 1995.

Manney, G., and J. L. Sabutis, Development of the polar vortex in the 1999–2000 Arctic winter stratosphere, *Geophys. Res. Lett.*, *27*, 2589–2592, 2000.

Mishchenko, M. I., Light scattering by randomly oriented axially symmetric particles, *J. Opt. Soc. Am. A Opt. Image Sci.*, *8*, 871–882, 1991.

Müller, R., and T. Peter, The numerical modelling of the sedimentation of polar stratospheric cloud particles, *Ber. Bunsen-Ges. Phys.*, *96*, 1992.

Naujokat, B., M. Kunze, and S. Pawson, Meteorology of the stratosphere during the THESEO2000/SOLVE winter: Evolution and evaluation, paper presented at THESEO2000/SOLVE Workshop, Eur. Comm., Palermo, Italy, Sept. 2000.

Pruppacher, H., and J. D. Klett, Microphysics of Clouds and Precipitation, 2nd ed., Kluwer Acad., Norwell, Mass., 1997.

Randel, W. J., et al., Seasonal cycles and QBO variations in stratospheric CH4 and H2O observed in UARS HALOE data, *J. Atmos. Sci.*, *55*, 163–185, 1998.

Rex, M., et al., Prolonged stratospheric ozone loss in the 1995–96 Arctic winter, *Nature*, *389*, 835–838, 1997.

Schiller, C., et al., Dehydration in the Arctic stratosphere during the THESEO2000/SOLVE campaigns, *J. Geophys. Res.*, *107*, 10.1029/2001JD000463, in press, 2002.

Schreiner, J., C. Voigt, A. Kohlmann, F. Arnold, K. Mauersberger, and N. Larsen, Chemical analysis of polar stratospheric cloud particles, *Science*, *283*, 968–970, 1999.

Shindell, D. T., D. Rind, and P. Lonergan, Increased polar stratospheric ozone losses and delayed eventual recovery owing to increasing greenhouse gas concentrations, *Nature*, *392*, 589–592, 1998.

Solomon, S., Progress towards a quantitative understanding of Antarctic ozone depletion, *Nature*, *347*, 347–354, 1990.

Solomon, S., et al., On the depletion of Antarctic ozone, *Nature*, *321*, 755–758, 1986.

Stowasser, M., H. Oelhaf, G. Wetzel, F. Friedl-Vallon, G. Maucher, M. Seefeldner, O. Trieschmann, T.v. Clarmann, and H. Fischer, Simultaneous measurements of HDO, H_2O, and CH_4 with MIPAS-B: Hydrogen budget and indication of dehydration inside the polar vortex, *J. Geophys. Res.*, *104*, 19,213–19,225, 1999.

Toon, B. O., P. Hamill, R. Turco, and J. Pinto, Condensation of HNO_3 and HCl in the winter stratospheres, *Geophys. Res. Lett.*, *13*, 1284–1287, 1986.

Toon, B. O., E. Browell, S. Kinneand, and J. Jordan, An analysis of lidar observations of polar stratospheric clouds, *Geophys. Res. Lett.*, *17*, 393–396, 1990.

Turco, R. P., R. C. Whitten, and O. B. Toon, Stratospheric aerosols: Observation and theory, *Rev. Geophys.*, *20*, 233–279, 1982.

Voigt, C., et al., Nitric acid trihydrate (NAT) in polar stratospheric clouds, *Science*, *290*, 1756–1758, 2000.
Vömel, H., et al., The evolution of the dehydration in the Antarctic stratospheric vortex, *J. Geophys. Res.*, *100*, 13,919–13,926, 1995.
Waibel, A. E., T. Peter, K. S. Carslaw, H. Oelhaf, G. Wetzel, P. J. Crutzen, U. Pschel, A. Tsias, E. Reimer, and H. Fischer, Arctic ozone loss due to denitrification, *Nature*, *283*, 2064–2069, 1999.
Wirth, M., and W. Renger, Evidence of large scale ozone depletion within the Arctic polar vortex 94/95 based on airborne lidar measurements, *Geophys. Res. Lett.*, *23*(8), 813–816, 1996.
Wirth, M., A. Tsias, A. Dörnbrack, V. Weiβ, K. S. Carslaw, M. Leutbecher, W. Renger, H. Volkert, and T. Peter, Model-guided Lagrangian observation and simulation of mountain polar stratospheric clouds, *J. Geophys. Res.*, *104*, 23,971–23,981, 1999.

A. Dörnbrack, A. Fix, H. Flentje, A. Meister, and H. Schmid, Institut für Physik der Atmosphäre, DLR Oberpfaffenhofen, D-82230 Wessling, Germany. (harald.flentje@dlr.de)
S. Füglistaler, B. Luo, and T. Peter, Laboratorium für Atmosphärenphysik, ETH Zürich, Ch-8093 Zürich, Switzerland.

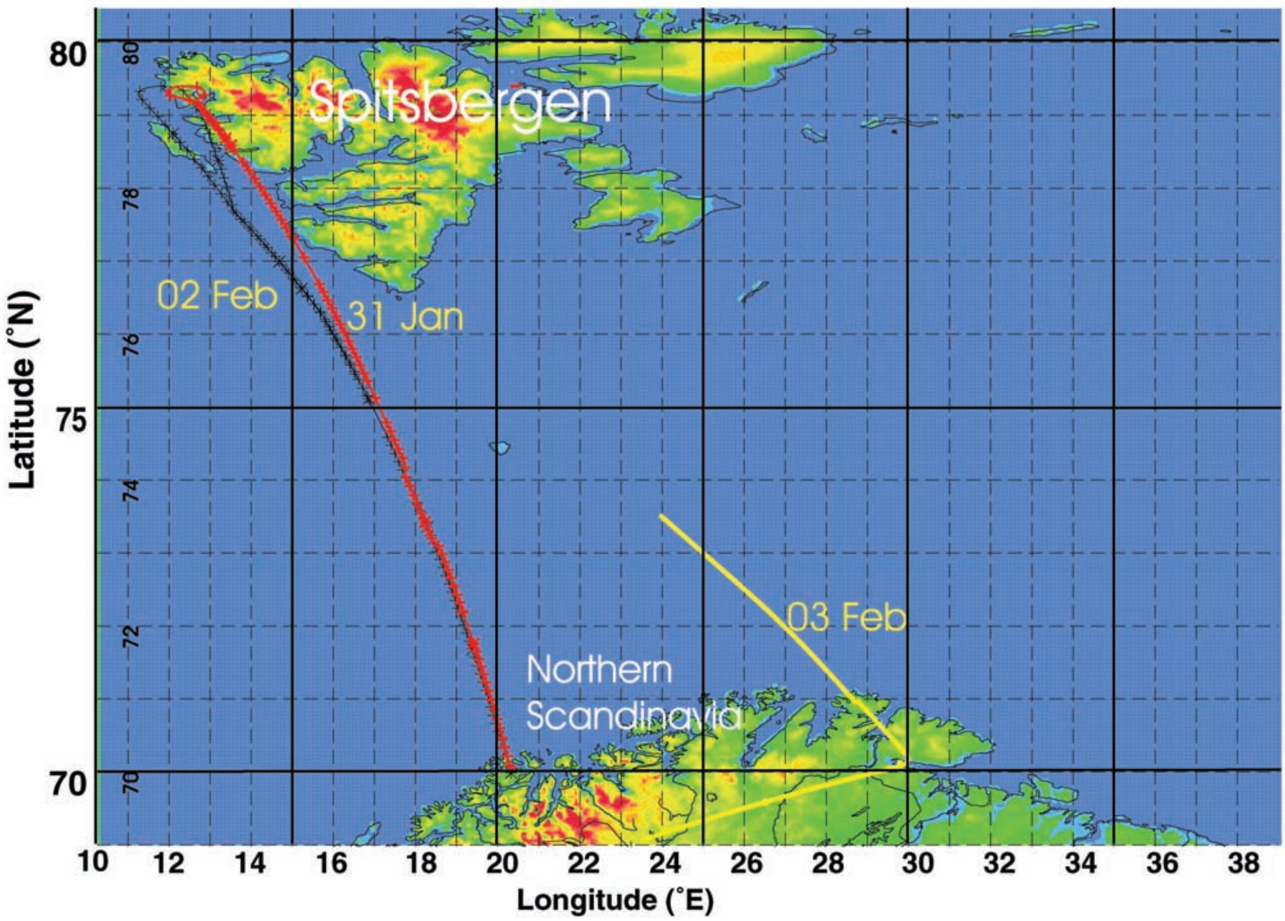

Figure 1. Falcon flight paths on 31 January 2000 (1030–1230 UT) and 2 February (1330–1505 UT) and 3 February 2000 (1940–2015 UT) over the Northern European Ice Sea south of Spitsbergen. Color-coded elevation shows peak altitudes of more than 1000 m above sea level.

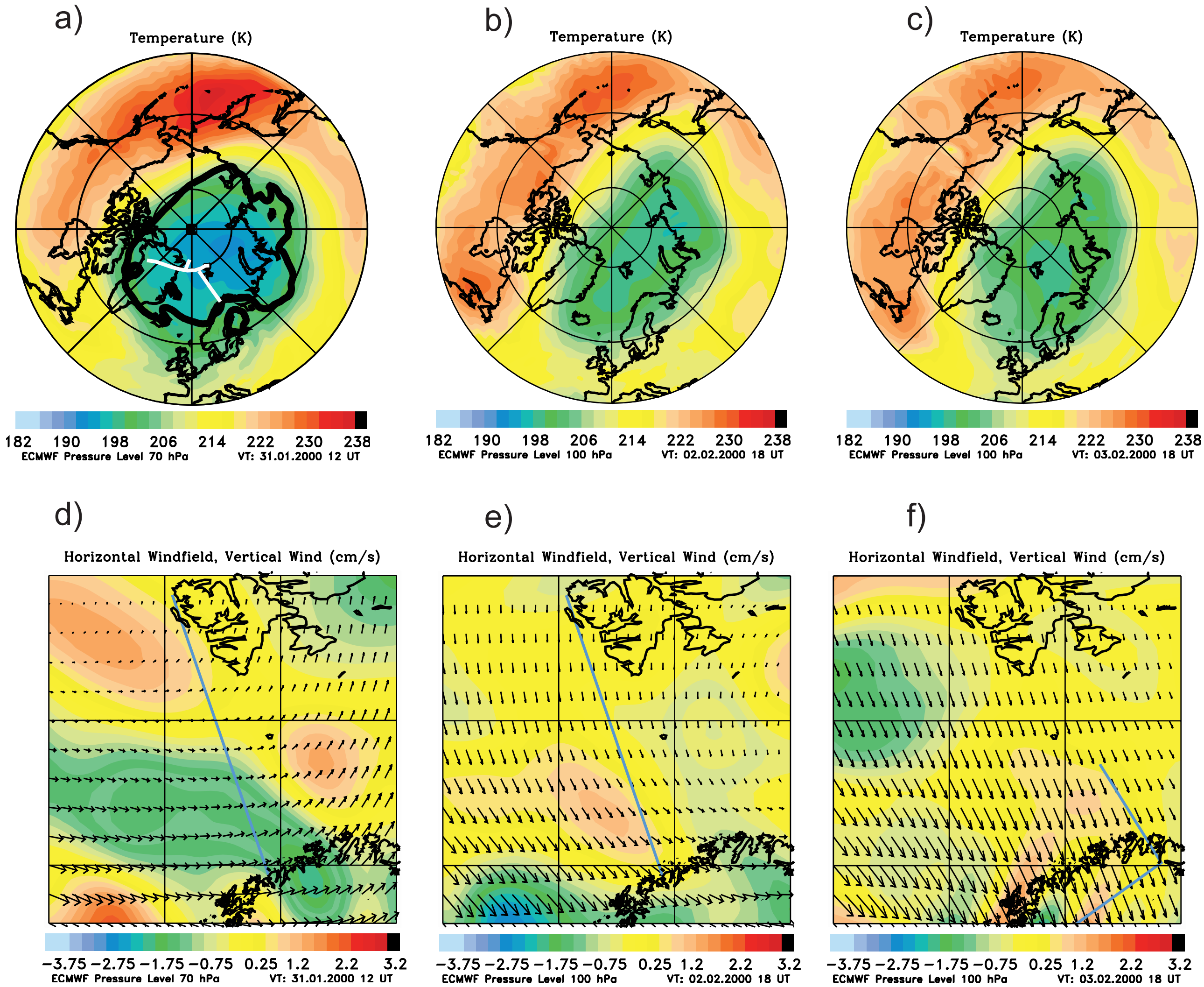

Figure 2. Upper panels: ECMWF temperatures at 70 hPa on (a) 31 January 1200 UT and at 100 hPa on (b) 2 February 1200 UT and (c) 3 February 1800 UT, corresponding to the respective central PSC levels. Color-coded temperatures range from 180 to 240 K. The vortex edge at 450 K is outlined by the 34 potential vorticity units (PVU) contour for 31 January. White lines in Figure 2a indicate the positions of the observed layers from 31 January, 2 and 3 February tracked back to 31 January, based on particle backward trajectories. Lower panels: Horizontal wind (arrows) and vertical wind (color-coded) from ECMWF analyses on (d) 31 January 1200 UT, (e) 2 February 1200 UT and (f) 3 February 1800 UT. The length of the arrows is proportional to the wind speed, whereby the longest arrows correspond to wind speeds of 6 m/s, 4.5 m/s and 2.5 m/s on 31 January, 2 and 3 February, respectively. Blue lines indicate the flight paths. The domain ranges from 68°N to 80°N and from 0°E to 30°E.

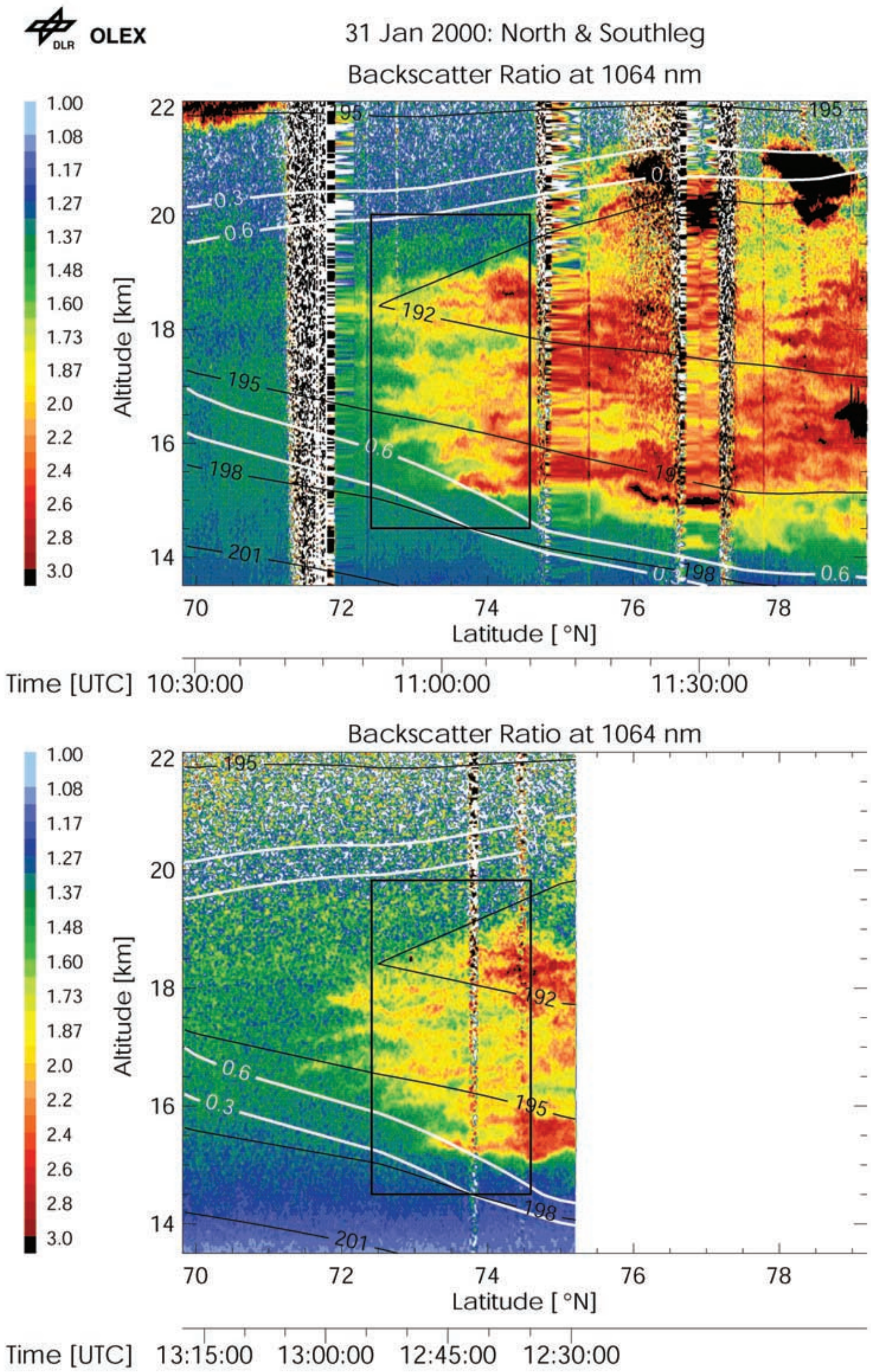

Figure 3. Backscatter ratio along the Falcon flight paths on 31 January 2000, not corrected for extinction, in order to maintain high spatial resolution. Each pair of panels shows the northward and southward legs of 2–3 hour turning point missions. Overlayed are contours of ECMWF temperature and of the fraction of HNO_3, which according to the phase diagram of *Hanson and Mauersberger* [1988] is in the (solid) NAT-phase, assuming 4.5 ppbv H_2O and a HNO_3 vertical column of 2.5×10^{20} m^{-2}. Noisy profiles result from strong extinction (shadowing) of the laser beam by cirrus clouds or are due to instrumental artifacts. The cloud section selected for the cross-covariance analysis is marked by a black frame.

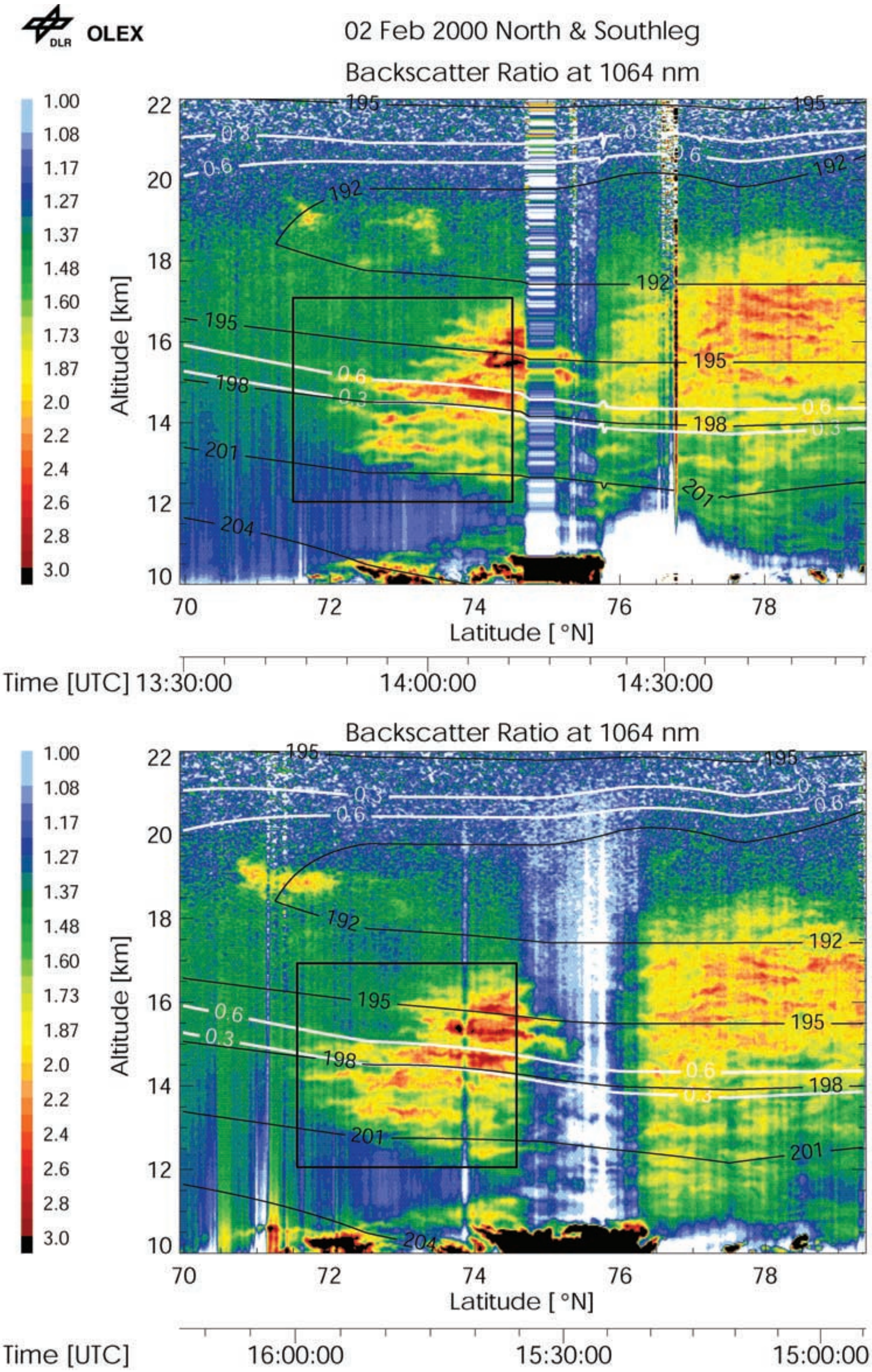

Figure 4. Backscatter ratio along the Falcon flight paths on 2 February as in Figure 3. The black (color-saturated) regions around 10.5 km altitude indicate strongly back-scattering cirrus clouds. In the PSC free region the volcanically produced BG-aerosol layer is evident below 20 km. The layers at that time already occurred at significantly lower altitudes than prescribed by the [NAT]/[HNO_3]-ratio isolines, which indicates denitrification at the upper levels and nitrification below (see text).

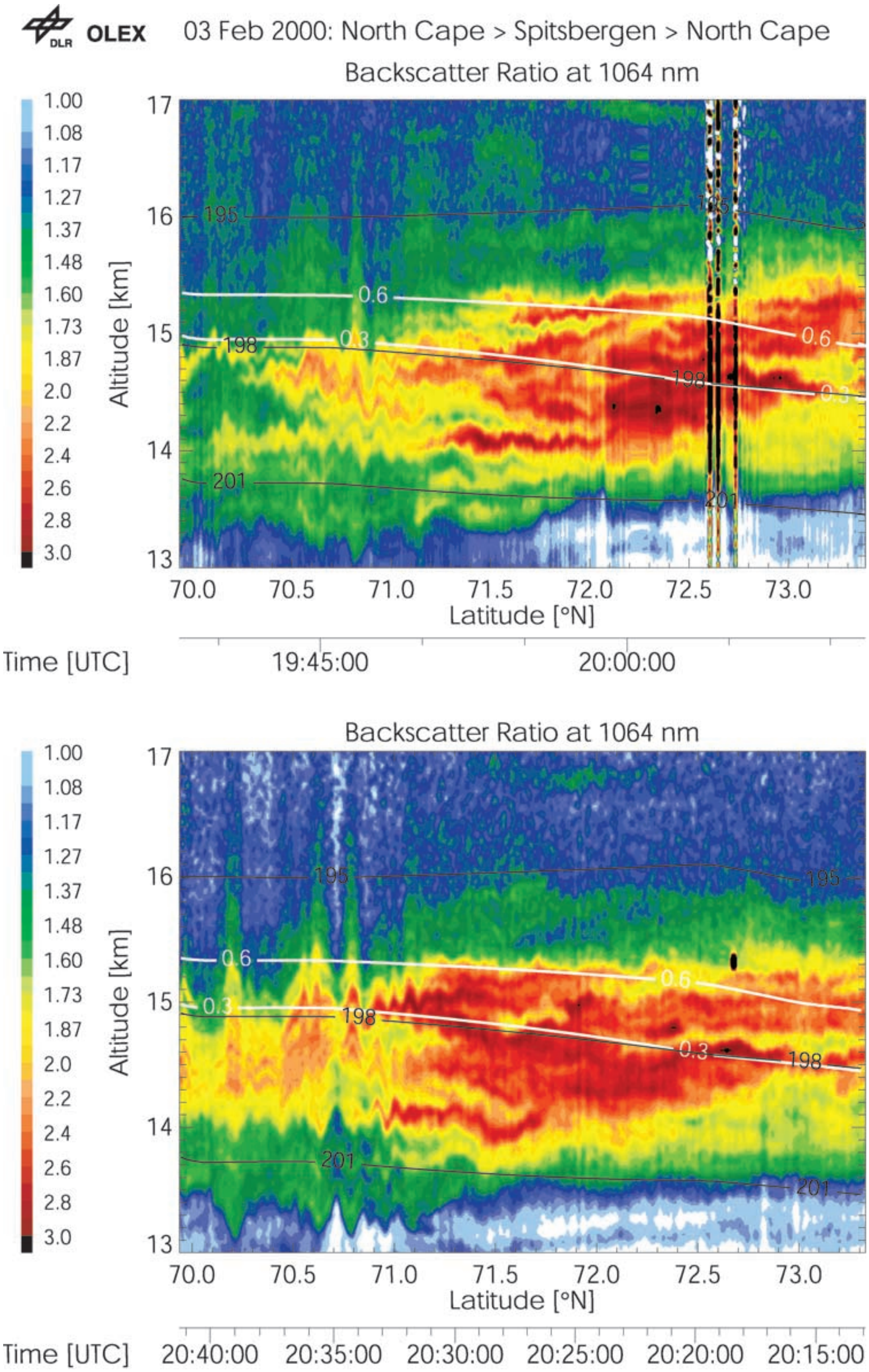

Figure 5. Backscatter ratio along the Falcon flight paths on 3 February as in Figure 3. The ER-2 contrail was observed at 2018 UTC near 72.7°N in 15.3 km. As compared to Figure 4 the denitrification/nitrification process had proceeded further.

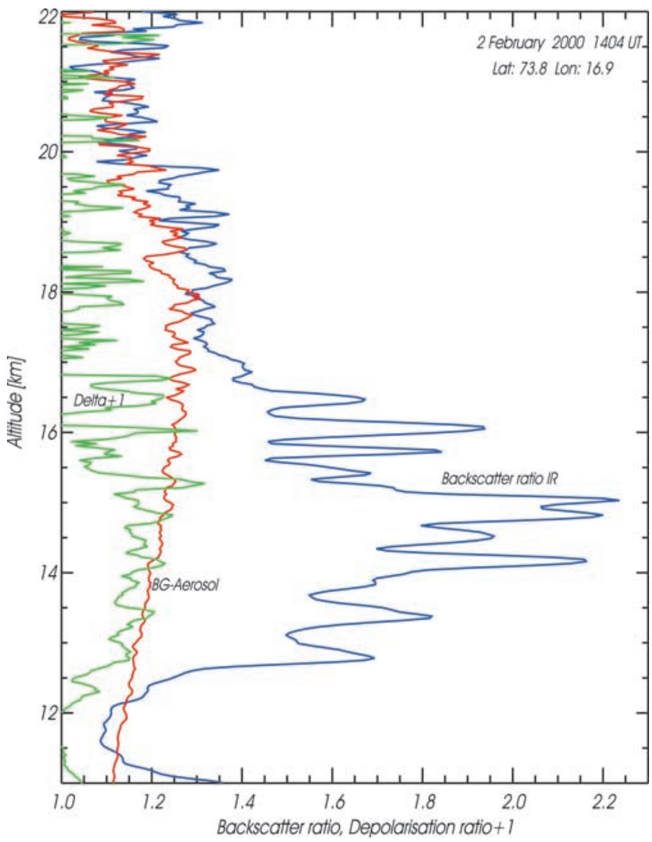

Figure 6. Profiles of total backscatter ratio γ_{1064} at 1064 nm (blue), background aerosol $\gamma_{BG,\ 1064}$ (red), particle depolarization ratio (corrected for contribution of background aerosol) δ_{532} at 532 nm (green) on 2 February 2000, 1404 UT.

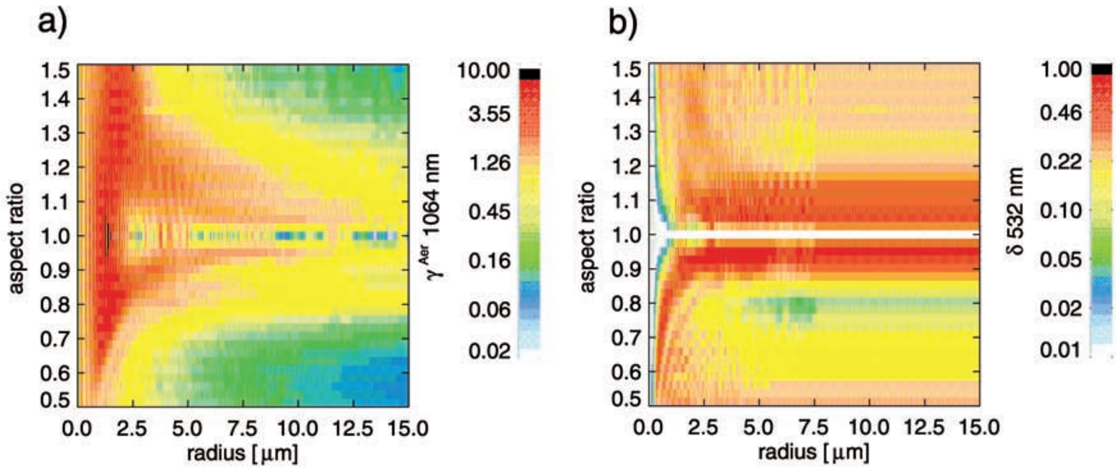

Figure 7. T-matrix calculations for spheroidal NAT particles with 1 ppbv condensed HNO_3: (a) Backscatter ratio at 1064 nm, (b) depolarization ratio at 532 nm. The backscatter ratio is proportional to the NAT particle mixing ratio. The particles are assumed to be lognormally distributed with a mode width of σ = 1.2.

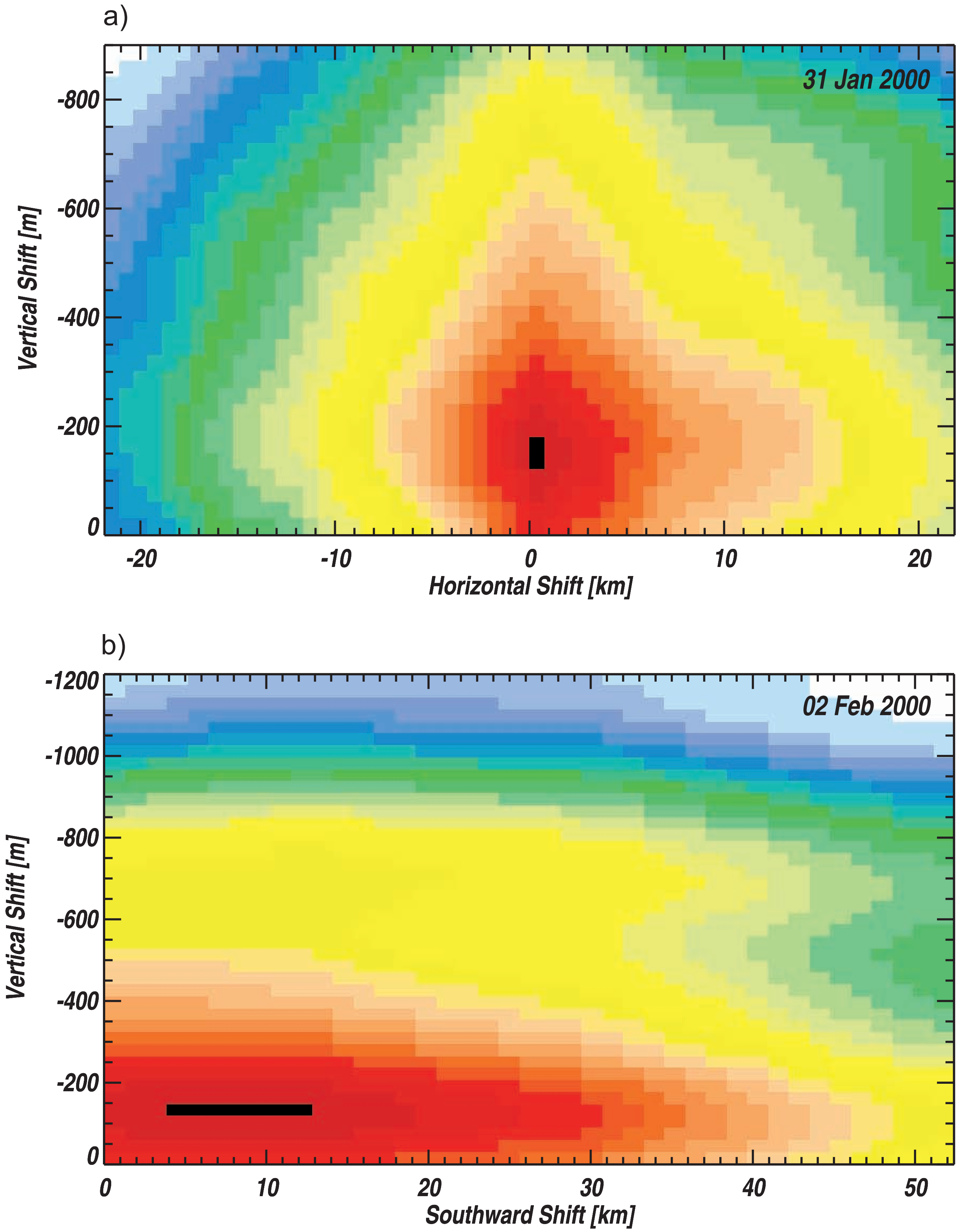

Figure 8. Covariance matrices for the horizontal and vertical shifts of selected backscatter ratio regions of the NAT layer PSCs on 31 January (a) and 2 February (b). The latitude/altitude sections cut for the analysis are [72.4°N to 73.7°N, 14.5–20 km] and [71.5°N to 74.6°N, 12–17 km] for 31 January and 2 February, respectively (compare Figures 3 and 4). Covariances are linearly rainbow color-coded in arbitrary units. The local maxima appear in black and indicate the shifts required for a best match of the selected data arrays.